One hole in a CuO_2 plane: Resonating-valence-bond-like behavior

M. W. Long and I. B. Styles
School of Physics and Astronomy, University of Birmingham, Birmingham, B15 2TT, United Kingdom
(Received 5 December 2003; revised manuscript received 14 June 2004; published 15 November 2004)

Although convincing arguments have been made which suggest that the three-band model of the high-T_c perovskite superconductors can be reduced to the single-band *t-J* model, there is a wealth of experimental data which indicates that this simplification may not be as valid as was first hoped. We perform variational and numerical calculations which demonstrate that in the absence of the Heisenberg interaction, the three-band model can provide a *low-spin* ground state, not the Nagaoka ferromagnetism predicted by the *t* model. We focus attention on the copper spin-spin correlations $\hat{S}_k$ and the oxygen hole occupation number $\hat{N}_k$ in order to provide evidence for or against long-range magnetic order and a Fermi discontinuity, respectively. The observed behavior appears similar to a Fermi liquid with a large Fermi surface, but there is no discontinuity in $\hat{N}_k$, and the system is clearly dominated by quantum spin fluctuations. A tendency to form spin dimers is seen, providing evidence for a *resonating valence bond* ground state.

DOI: 10.1103/PhysRevB.70.205119 PACS number(s): 71.10.Fd, 71.10.Hf

I. INTRODUCTION

The emergence of superconductivity upon doping some antiferromagnetic Mott insulators remains one of the least-well-understood problems in condensed matter physics, despite the vast amount of activity in the field. A variety of possible mechanisms have been proposed: a single hole moving in a Mott antiferromagnet,[1] spin bags,[2] the interaction between pairs of holes moving in an itinerant antiferromagnet,[3] phase separation (stripes),[4] and bipolarons[5] are among the many proposals. These ideas are often extremely sophisticated and can sometimes require uncontrolled assumptions to be made. In this paper, we extend previous work[6] on a simple model which does not require such assumptions, and we demonstrate that this model displays some of the basic physical phenomena present in the high-T_c superconductors at the level of a single hole doped into a CuO_2 plane. Even the apparently straightforward one-hole limit requires considerable sophistication to investigate adequately, and we do not attempt to study the interaction between charge carriers which may lead to superconductivity. We also choose to ignore the superexchange interaction, preferring instead to focus on the correlations induced by the motion of the hole. The two fundamental questions we address are, is the system a Fermi liquid, and how does the motion of the hole lift the spin degeneracy?

The reduction of the natural three-band model arising from the solid-state chemistry of the cuprates to the single-band *t-J* model[1] has led to an intense but largely unsuccessful effort to explain the physical properties of the high-T_c superconductors within the one-band framework. In this work, we demonstrate that the *t-J* model leads to a very different ground state to the natural three-band model, and this provides a possible explanation for the asymmetry of the phase diagram with regard to electron versus hole doping.

We commence by introducing the model under consideration. The three-band model for holes in the CuO_2 planes is[7]

$$\mathcal{H} = -\Delta \sum_{i\sigma} d^{\dagger}_{i\sigma} d_{i\sigma} + U \sum_{i} d^{\dagger}_{i\uparrow} d_{i\uparrow} d^{\dagger}_{i\downarrow} d_{i\downarrow} + V \sum_{\langle ij\rangle\sigma} (d^{\dagger}_{i\sigma} p_{j\sigma} + p^{\dagger}_{j\sigma} d_{i\sigma}) - t_{\mathrm{p}} \sum_{\langle jj'\rangle\sigma} p^{\dagger}_{j\sigma} p_{j'\sigma}, \quad (1)$$

where $d^{\dagger}_{i\sigma}$ creates a hole of spin σ on copper site i in the $3d_{x^2-y^2}$ orbital, and $p^{\dagger}_{j\sigma}$ does likewise for the oxygen $2p_x$, $2p_y$ orbitals illustrated in Fig. 1.

We have chosen to make all neighboring copper and oxygen states bonding which is equivalent to translating reciprocal space by (π, π). All energies and matrix elements are expected to be positive. In the ground state of the parent compounds there is a single hole in the $3d_{x^2-y^2}$ orbital on every copper site (giving Cu^{2+}, $3d^9$), and the oxygen states are filled (O^{2-}, $2p^6$). Upon hole doping, the extra holes enter the planes in the oxygen $2p_x$, $2p_y$ orbitals, and hence any treatment of this model is constrained by single occupancy of the copper sites. The approximate values of the energy scales involved can be obtained from experiment, where one can naturally use J, the superexchange coupling;[8–13] J_C, the cyclic exchange energy;[14] W, the single-hole bandwidth;[15] and Δ_{opt}, the optical gap[16] to constrain the values of these parameters. This does not unambiguously provide the energy

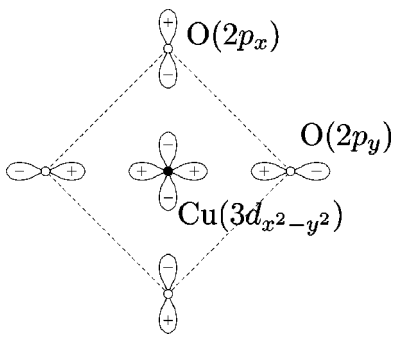

FIG. 1. A single copper-oxygen "plaquette" showing the orbitals involved in hybridization.

scales, but most of the experiments are explained by the following choice. The first two terms of Eq. (1) operate on energy scales of $\Delta \approx 2$ eV and $U \approx 10$ eV, respectively, and this provides the Mott restriction of single occupancy, while the third term operates on a scale $V \approx 0.75$ eV, and this lifts the copper spin degeneracy at second order. Since the material is a known Mott insulator, we may treat the hybridization V as a perturbation to the atomic physics, and employing a canonical transformation[17] lifts the spin degeneracy and provides the effective Hamiltonian

$$\mathcal{H}_{\text{eff}} = X \sum_{\langle ij \rangle \sigma} \sum_{\langle ij' \rangle \sigma'} d^{\dagger}_{i\sigma} p^{\dagger}_{j\sigma'} p_{j'\sigma} d_{i\sigma'} - t \sum_{\langle ij \rangle \sigma} \sum_{\langle ij' \rangle} p^{\dagger}_{j\sigma} p_{j'\sigma} - t_{\text{p}} \sum_{\langle jj' \rangle \sigma} p^{\dagger}_{j\sigma} p_{j'\sigma} \tag{2}$$

under the constraint of single copper occupancy. Note the absence of the index i in the summand of the second term, although it is summed over. This corresponds to a hole being allowed to hop from one oxygen site to *any* other oxygen site on the same plaquette. The sum is then over the neighbors of the copper ion, not the neighbors of the oxygen ion, and so second-neighbor oxygen hopping is also included here. The energy scales are $X = UV^2/\Delta(U-\Delta)$ and $t = V^2/(U-\Delta)$, and the associated terms display distinct behavior. The first term moves the oxygen hole on a plaquette, exchanging its spin with the associated copper hole. The second term hops the oxygen hole on the plaquette, but does not exchange the spins.

The presence of direct oxygen-oxygen hopping via t_{p} complicates matters somewhat. This amounts to an anisotropic reparametrization of the second term of Eq. (2), which includes both first- and second-neighbor hopping of oxygen states, since the hole hops to all sites with which it shares a copper site. In addition, this term prevents the reduction of Eq. (1) to a Kondo lattice model, by preventing the exact decoupling of bonding and nonbonding states. In practical terms, the inclusion of t_{p} adds unnecessary complexity to the model, and we set $t_{\text{p}} = 0$, choosing to study the competition between the energy scales t and X only. Physically, a careful analysis of the signs of the interactions reveals that setting $t_{\text{p}} > 0$ (the physical assumption) corresponds to an increase in t, which is equivalent to a reduction in $U - \Delta$. This favors the fluctuation $Cu^{2+} \mapsto Cu^{3+}$ (for which there is no experimental evidence[18,19]) instead of the $Cu^{2+} \mapsto Cu^{+}$ fluctuations favored in the large-U limit.

For a single hole, we can identify two exact solutions of the model. Employing the operators

$$\hat{A}_i = \frac{1}{Z} \sum_{\langle ij \rangle \sigma} \sum_{\langle ij' \rangle \sigma'} d^{\dagger}_{i\sigma} d_{i\sigma'} p^{\dagger}_{j'\sigma'} p_{j\sigma}, \tag{3}$$

,

$$\hat{B}_i = \frac{1}{Z} \sum_{\langle ij \rangle \sigma} \sum_{ij'} p^{\dagger}_{j'\sigma} p_{j\sigma} \tag{4}$$

(where Z is the coordination number of the lattice), it is easy to show that in the subspace restricted to a single oxygen hole,

$$\hat{A}_i \hat{A}_i = \hat{B}_i, \quad \hat{A}_i \hat{B}_i = \hat{A}_i,$$

$$\hat{B}_i \hat{A}_i = \hat{A}_i, \quad \hat{B}_i \hat{B}_i = \hat{B}_i,$$

and consequently that

$$\hat{s}_i = \frac{1}{2}(\hat{B}_i - \hat{A}_i), \quad \hat{t}_i = \frac{1}{2}(\hat{B}_i + \hat{A}_i) \tag{5}$$

are projection operators onto the antisymmetric and symmetric subspaces, respectively. The singlet

$$S^{\dagger}_{ij} = \frac{1}{\sqrt{2}} \sum_{\sigma} \sigma d^{\dagger}_{i\sigma} p^{\dagger}_{j\bar{\sigma}} \tag{6}$$

and triplet

$$T^{1\dagger}_{ij} = d^{\dagger}_{i\uparrow} p^{\dagger}_{j\uparrow},$$

$$T^{0\dagger}_{ij} = \frac{1}{\sqrt{2}} \sum_{\sigma} d^{\dagger}_{i\sigma} p^{\dagger}_{j\bar{\sigma}}, \tag{7}$$

$$T^{\bar{1}\dagger}_{ij} = d^{\dagger}_{i\downarrow} p^{\dagger}_{j\downarrow}$$

operators allow the model to be represented as

$$\mathcal{H} = Z(X - t) \sum_i \hat{t}_i - Z(X + t) \sum_i \hat{s}_i, \tag{8}$$

where

$$\hat{t}_i = \frac{1}{Z} \sum_{\alpha} \sum_{\langle ij \rangle} T^{\alpha\dagger}{}_{ij} \sum_{\langle ij' \rangle} T^{\alpha}{}_{ij'}, \tag{9}$$

$$\hat{s}_i = \frac{1}{Z} \sum_{\langle ij \rangle} S^{\dagger}_{ij} \sum_{\langle ij' \rangle} S_{ij'}. \tag{10}$$

These two terms can be isolated by the choice of parameters $t = \pm X$, providing two exactly solvable limits.

The first exact solution is found by setting $t = -X$, corresponding to the unphysical limit $U = -\Delta$. The model here is sum of triplet projectors and so has a positive-definite spectrum. The ground-state manifold is large and consists of states when all the projection operators have vanishing eigenvalues, yielding zero total energy. This can occur in one of two ways: the oxygen hole is in a *singlet* with its neighbor, or the hole wave function has zero average weight (i.e., is in a nonbonding orbital). From these ideas we can construct a large number of ground states with a variety of properties. This task is simplified greatly by noting that solutions for the linear one-dimensional chain are also valid solutions of the two-dimensional system: *a nonbonding orbital in one dimension remains a nonbonding orbital in two dimensions, since the phase cancellation stops motion onto the perpendicular atoms as well*. The linear chain can trace any path in the plane provided that any loops may only be traversed in one direction.

Consider first the possibility of local spin singlets. Representing a singlet using the common notation

$$|S_{ij}\rangle = \underset{i\quad j}{(\times\ \times)}, \tag{11}$$

and noting that a hole cannot be in a singlet with both neighbors simultaneously, we observe that

$$|S_{ij}\rangle = \cdots (\times\ h)(\times\ \cdot\ \times)\cdots - \cdots (\times\ \cdot\ \times)(h\ \times)\cdots \tag{12}$$

is a ground state of the full lattice, where $\times$ indicates a copper site, h is the oxygen hole, and $\cdot$ is a filled-shell oxygen site. The hole is in a singlet when neighboring either of the outer copper spins and cannot interact with them. Projecting the hole and the central spin onto a triplet yields the same state for both configurations, and the choice of phase means this is a *nonbonding* configuration. The more general state which allows the hole to delocalize freely (in the above state, the hole is localized to the central copper site) can be constructed by analogy quite easily, and we obtain

$$\begin{aligned}|\psi\rangle = {} & + \cdots (\times\ h)(\times\ \cdot\ \times)\ \cdot\ (\times\ \cdot\ \times)\cdots \\ & - \cdots (\times\ \cdot\ \times)(h\ \times)\ \cdot\ (\times\ \cdot\ \times)\cdots \\ & - \cdots (\times\ \cdot\ \times)\ \cdot\ (\times\ h)(\times\ \cdot\ \times)\cdots \\ & + \cdots (\times\ \cdot\ \times)\ \cdot\ (\times\ \cdot\ \times)(h\ \times)\cdots \\ & + \cdots ,\end{aligned} \tag{13}$$

where the phases are chosen to provide locally bonding states or Zhang-Rice singlets. Such states are particularly useful as they allow the hole to delocalize without incurring a penalty from the formation of triplet states.

We may also identify a second class of ground state. The states

$$|\psi_1\rangle = \left\{ \begin{array}{l} \overset{h}{+\ \cdots\ \sigma_0\ \sigma_1\ \sigma_2\ \cdot\ \sigma_3\ \cdot\ \sigma_4\ \cdots} \\ \overset{h}{+\ \cdots\ \sigma_0\ \sigma_2\ \sigma_1\ \cdot\ \sigma_3\ \cdot\ \sigma_4\ \cdots} \\ \overset{h}{-\ \cdots\ \sigma_0\ \cdot\ \sigma_1\ \sigma_2\ \sigma_3\ \cdot\ \sigma_4\ \cdots} \\ \overset{h}{-\ \cdots\ \sigma_0\ \cdot\ \sigma_2\ \sigma_1\ \sigma_3\ \cdot\ \sigma_4\ \cdots} \end{array} \right\}, \tag{14}$$

$$|\psi_2\rangle = \left\{ \begin{array}{l} \overset{h}{+\ \cdots\ \sigma_0\ \sigma_1\ \sigma_2\ \cdot\ \sigma_3\ \cdot\ \sigma_4\ \cdots} \\ \overset{h}{-\ \cdots\ \sigma_0\ \sigma_2\ \sigma_1\ \cdot\ \sigma_3\ \cdot\ \sigma_4\ \cdots} \end{array} \right\}, \tag{15}$$

$$|\psi_3\rangle = \left\{ \begin{array}{l} \overset{h}{+\ \cdots\ \sigma_0\ \cdot\ \sigma_1\ \sigma_2\ \sigma_3\ \cdot\ \sigma_4\ \cdots} \\ \overset{h}{-\ \cdots\ \sigma_0\ \cdot\ \sigma_2\ \sigma_1\ \sigma_3\ \cdot\ \sigma_4\ \cdots} \end{array} \right\} \tag{16}$$

(where h labels the oxygen hole and $\cdot$ indicates an unoccupied oxygen site) are all eigenstates of the triplet operator, whatever the choice of spins σ_i. The state $|\psi_1\rangle$ is a triplet in a nonbonding orbital, and $|\psi_2\rangle$, $|\psi_3\rangle$ are local singlets. These two ideas can be combined to form two new *local* ground states:

$$|\psi_n\rangle = \begin{array}{l} \overset{h}{+\ \cdots\ \sigma_0\ \sigma_1\ \sigma_2\ \cdot\ \sigma_3\ \cdot\ \sigma_4\ \cdots} \\ \overset{h}{-\ \cdots\ \sigma_0\ \cdot\ \sigma_2\ \sigma_1\ \sigma_3\ \cdot\ \sigma_4\ \cdots} \end{array} \tag{17}$$

has the hole hopping in a pure nonbonding orbital, while

$$|\psi_t\rangle = \begin{array}{l} \overset{h}{+\ \cdots\ \sigma_0\ \sigma_1\ \sigma_2\ \cdot\ \sigma_3\ \cdot\ \sigma_4\ \cdots} \\ \overset{h}{-\ \cdots\ \sigma_0\ \cdot\ \sigma_1\ \sigma_2\ \sigma_3\ \cdot\ \sigma_4\ \cdots} \end{array} \tag{18}$$

has the hole hopping via the translation of a *pair* of spins such that the spin order is preserved. These local solutions are readily generalized, providing

$$|\psi_N\rangle = \begin{array}{l} \overset{h}{+\ \cdots\ \sigma_0\ \sigma_1\ \sigma_2\ \cdot\ \sigma_3\ \cdot\ \sigma_4\ \cdots} \\ \overset{h}{-\ \cdots\ \sigma_0\ \cdot\ \sigma_2\ \sigma_1\ \sigma_3\ \cdot\ \sigma_4\ \cdots} \\ \overset{h}{+\ \cdots\ \sigma_0\ \cdot\ \sigma_2\ \cdot\ \sigma_3\ \sigma_1\ \sigma_4\ \cdots} \end{array} \tag{19}$$

and

$$|\psi_B\rangle = \begin{array}{l} \overset{h}{+\ \cdots\ \sigma_0\ \sigma_1\ \sigma_2\ \cdot\ \sigma_3\ \cdot\ \sigma_4\ \cdots} \\ \overset{h}{-\ \cdots\ \sigma_0\ \cdot\ \sigma_1\ \sigma_2\ \sigma_3\ \cdot\ \sigma_4\ \cdots} \\ \overset{h}{+\ \cdots\ \sigma_0\ \cdot\ \sigma_1\ \cdot\ \sigma_2\ \sigma_3\ \sigma_4\ \cdots} \end{array} . \tag{20}$$

The solutions provided at $t=-X$ have full spin degeneracy which is lifted as we perturb away from this point. We can apply second-order degenerate perturbation theory to show that the first type of solution, the nonbonding state, is most relevant at $t<-X$, well away from the real physical limit, but the second type is an excellent picture of what we believe to occur in the system and provides us with some physical intuition for the behavior of the system when $t>-X$. The nonbonding state does not lift the degeneracy, but in the states where the motion preserves the spin order, the singlet interaction stabilizes the Heisenberg ground state. In Sec. IV we numerically solve the t-X model very close to $t=-X$ (the limit itself cannot be solved uniquely due to the degeneracy), and we find that the resulting ground state is essentially that of the nearest-neighbor Heisenberg model (see Fig. 12), with the hole motion described by Eq. (20). This is consistent with our observations in this section.

In the second natural limit, $t=X$ corresponding to $\Delta=U$, the model is expressed in terms of the singlet projectors only. Since the sign of the coefficient is negative, the ground state is reached when the projection operators have their maximum eigenvalues. This maximum (unity) is reached when the hole spin and copper spin are in a local singlet, and the hole is simultaneously in a pure *bonding* configuration, a Zhang-Rice singlet.[1] Clearly this cannot be achieved on neighboring copper sites as the oxygen hole cannot be in a singlet with both copper spins simultaneously.

The action of the Hamiltonian preserves Zhang-Rice singlets, and hence one can represent the system on the copper sublattice only in terms of the states

$$\prod_{i\neq i'} c^{\dagger}_{i\sigma_i}|0\rangle \equiv \sum_{j\in\{i'\}} S^{\dagger}_{i'j}\prod_{i\neq i'} d^{\dagger}_{i\sigma_i}|0\rangle, \tag{21}$$

where the operator $S^{\dagger}_{ij}$ creates a local copper- (i-) oxygen (j) singlet, and the sum over $j\in\{i'\}$ implies summing over the oxygen neighbors, j of copper site i'. This provides the effective Hamiltonian

$$\mathcal{H} = -2Zt_{\mathrm{h}}\sum_{i\sigma} c_{i\sigma}c^{\dagger}_{i\sigma} - t_{\mathrm{h}}\sum_{\langle ii'\rangle\sigma} c_{i\sigma}c^{\dagger}_{i'\sigma} + U\sum_{i} c^{\dagger}_{i\uparrow}c_{i\uparrow}c^{\dagger}_{i\downarrow}c_{i\downarrow}, \tag{22}$$

where U is the Coulomb repulsion and t_{h} is the effective hopping energy of the Zhang-Rice singlet between adjacent copper sites. The limit $U\mapsto\infty$ restricts the system to single occupancy, yielding the one-band model. Once again, the background spin configuration remains exactly degenerate, but this is lifted as we perturb away from $t=X$. The limit $t>X$ provides a ferromagnetic background while $t<X$ provides the Heisenberg ground state. The dominant contribution of the Zhang-Rice singlet near to this limit is verified by the numerical calculations presented in Fig. 12 and the surrounding discussion. This is an exact mapping for a single hole, and the model is exactly solvable in this limit on the square lattice at $U=\infty$: the Nagaoka problem,[20] providing a ferromagnetic ground state. There is no experimental evidence for such a phase in the cuprate superconductors; indeed, at the level of a single hole the ground state is strongly antiferromagnetic. In order to destabilize the ferromagnetism the weaker antiferromagnetic Heisenberg interaction arising from superexchange must be included, leading to the widely studied t-J model,

$$\mathcal{H} = -t_{\mathrm{h}}\sum_{\langle ii'\rangle\sigma} c_{i\sigma}c^{\dagger}_{i'\sigma} + \frac{J}{2}\sum_{\langle ii'\rangle}\mathbf{S}_i\cdot\mathbf{S}_{i'} + U\sum_{i} c^{\dagger}_{i\uparrow}c_{i\uparrow}c^{\dagger}_{i\downarrow}c_{i\downarrow}, \tag{23}$$

with single occupancy again enforced by $U=\infty$. There is hence a competition between the Nagaoka tendency toward ferromagnetism and the Heisenberg interaction which desires long-range magnetic order. In the undoped case this model is a pure Heisenberg antiferromagnet, and one would expect the addition of holes to destroy the antiferromagnetism. The phase diagram of the single-layer cuprates indicates that this phase is destroyed by surprisingly small concentrations of holes and is replaced by the superconducting phase. This leads one to conclude that the energy of the hole motion destroys the long-range correlations favored by the antiferromagnetic J, suggesting that the t model describes this situation correctly. This is certainly true at $\Delta=U$, where the three-band model reduces exactly to the one-band model, but provides a ferromagnetic state which is not seen experimentally (where $\Delta\gtrsim 0.2U$). One must either include a dominant antiferromagnetic interaction or study a model in which the charge motion stabilizes the observed low-spin ground state in the one-hole limit. In this article, we provide evidence that such behavior may be observed in the t-X model [Eq. (2)].

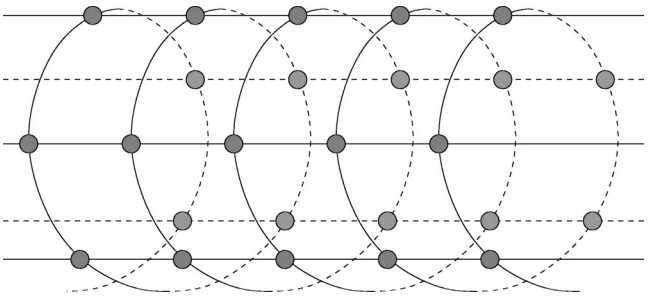

FIG. 2. An example spiral geometry, with "pitch" $p=5$.

II. METHODOLOGY

We have chosen to study a single hole on the CuO_2 square lattice using the scaling properties of finite systems. The difficulties involved in scaling pure two-dimensional systems are such that we have elected to study one-dimensional scaling, followed by the scaling of a sequence of one-dimensional systems which limit to the desired two-dimensional system. Such an approach has inherent difficulties: one-dimensional systems are pathological and are almost always spin-charge-separated Luttinger liquids; hence, great care is required. However, such an approach offers useful simplifications: the associated variables are one dimensional and so are much easier to handle exhaustively.

The geometries that we study in this work are perhaps best represented as *spirals*, as shown in Fig. 2.

This is exactly equivalent to the linear chain with additional pth-neighbor bonds, and in the limit $N\mapsto\infty$, $p\mapsto\infty$ (where N is the number of sites in the chain), this geometry tends toward the square lattice (as long as N/p remains finite). The Brillouin zone for these systems maps onto a line which crosses the square-lattice Brillouin zone p times in one direction as the zone is traversed in the orthogonal direction, as shown in Fig. 3.

Our representation then implies that the two-dimensional reciprocal lattice vector $\mathbf{k}=(k_x,k_y)$ is subject to the restriction $k_x/k_y=\mathrm{const}$, and so we can use a scalar representation k. Notice that the simple free-electron picture predicts that these systems will have a complicated multipart "Fermi volume." For large values of p, the one-dimensional behavior becomes very complex and extracting the two-dimensional character from the scaling data requires great care.

One complication that results from this choice of geometry is the nature of the boundary conditions. One can envisage the spiral connected as a *torus* if we choose to have closed boundary conditions (a natural choice), and this creates two sets of boundary conditions. The most obvious is the choice of periodic versus antiperiodic boundary conditions around the whole system, equivalent to the inclusion of a flux through the center of the torus. There is also a choice of phase inherent in moving once around a segment of the spiral, and one can also have periodic-antiperiodic boundary conditions around this loop, equivalent to the inclusion of a

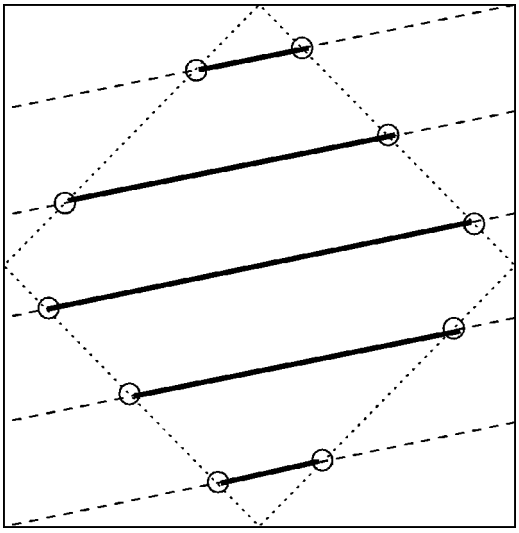

FIG. 3. The reciprocal-space representation of the $p=5$ spiral.

flux through the center of the spiral. When dealing with finite systems, one must consider all four possible combinations of boundary conditions. Only in the thermodynamic limit do the boundary conditions become equivalent, and we will use this fact to judge whether a given system is representative of this limit. We will discuss this issue in more detail in Sec. IV.

The two issues which we will investigate in this work are rather fundamental to the understanding of the basic nature of high-temperature superconductivity (HTS): the magnetic ordering induced by motion of a hole and Fermi liquid behavior. The first issue is important since the most popular model of HTS is the *t-J* model, which predicts that a single hole will induce ferromagnetism in the absence of superexchange, while the second issue may be important in helping to understand recent experiments[21] which have observed possible non-Fermi-liquid behavior in the cuprates. We investigate these issues using two analogous procedures.

The natural quantity to consider with regard to the magnetism is

$$\hat{S}_n = \frac{1}{N}\sum_i \hat{\mathbf{S}}_i \cdot \hat{\mathbf{S}}_{i+n}, \tag{24}$$

for a translationally invariant system, with the associated reciprocal-space operator

$$\hat{S}_k = \sum_n \mathrm{e}^{-\mathrm{i}kR_n}\hat{S}_n. \tag{25}$$

These operators are of direct relevance to elastic magnetic neutron scattering, and the Bragg spots which correspond to long-range order are described by a peak in $\hat{S}_k$ at $k=k^*$, which diverges linearly with system size. The presence of a Bragg spot tells us that all spins are involved and are correlated in a spiral with pitch k^*. These operators are subject to the constraint $(1/N)\Sigma_{\mathbf{k}}\hat{S}_{\mathbf{k}}=s(s+1)=\frac{3}{4}$, and at most $\frac{1}{3}$ of this is contributed by the Bragg spot. This is illustrated by the analytic form of $\hat{S}_{\mathbf{k}}$ for the classical spin-half Neél state on the square lattice:

$$\hat{S}_{\mathbf{k}} = \frac{1}{2} - \frac{1}{2}\delta_{\mathbf{k0}} + \left(\frac{1}{2}+\frac{N}{4}\right)\delta_{\mathbf{kQ}}, \tag{26}$$

where it is easily shown that the contribution to S_0 from the Bragg spot $\mathbf{k}=\mathbf{Q}$ is $S_0/3=\frac{1}{4}$. The remainder of the spin density is contributed by a short-range background state. In the forthcoming numerical calculations (Sec. IV), the Bragg spot (long-range order) shows up as a peak which diverges with system size, whereas the short-range background is well converged.

The corresponding operators for investigating Fermi-liquid behavior are

$$\hat{N}_n = \frac{1}{N}\sum_{j\sigma} p^{\dagger}_{i,\sigma}p_{i+n,\sigma} \tag{27}$$

for a translationally invariant system, with the resulting transform

$$\hat{N}_k = \frac{1}{N}\sum_n \mathrm{e}^{-\mathrm{i}\mathbf{k}\cdot\mathbf{R}_n}\hat{N}_n. \tag{28}$$

The interpretation of these quantities is subtle and requires some explanation. First of all we note that although the cuprates are Mott insulators at zero doping, suggesting that they are half-filled, this is only true with regard to the Cu^{2+} band. In the parent compounds, the oxygen bands are empty. When we add a single oxygen hole to the system, the occupation number $\hat{N}_k$ is equal to $\delta\hat{N}_k$ which is the *change* in occupation number as the hole is added not to a half-filled band, but to an empty band. For a Fermi gas, this provides a δ-function peak at the Fermi level when a single hole is added: the occupation is discontinuous between full and empty at $T=0$. In finite systems one would expect $\hat{N}_{k_\mathrm{F}}=1$, since one is adding a single hole. In the case of an interacting Fermi liquid, there is still a discontinuity at the Fermi level, but with a reduced height $Z_{\mathbf{k}}$. A finite fraction of the hole is placed at the Fermi point, and the remainder is spread smoothly over the rest of the Brillouin zone. For a single particle, $\Sigma_{\mathbf{k}}\hat{N}_k=1$, and so the height of the peak at the Fermi point is *reduced* as N increases as the weight of the single particle is spread over N k points. It is therefore useful to normalize $\hat{N}_k$, and in practice we actually calculate $N\hat{N}_k$. We will see that this allows us to isolate the discontinuity at the Fermi level as a peak which diverges with system size indicating long-range order, set against a background of short-range correlations which converge. The rate at which the peak diverges provides a signature for Fermi-liquid behavior: for both interacting and noninteracting Fermi liquids, $N\hat{N}_{k_\mathrm{F}} \sim N$, while for Luttinger liquids, $N\hat{N}_{k_\mathrm{F}} \sim N^{\alpha}$, where $0<\alpha<1$.

The behavior of the peak at the Fermi level thus provides us with a characteristic signature for Fermi liquid behavior. Short-range correlations will converge with system size, whereas the long-range correlations which characterize Fermi and Luttinger liquids will be seen as a peak at the Fermi level. If the peak diverges linearly with system size,

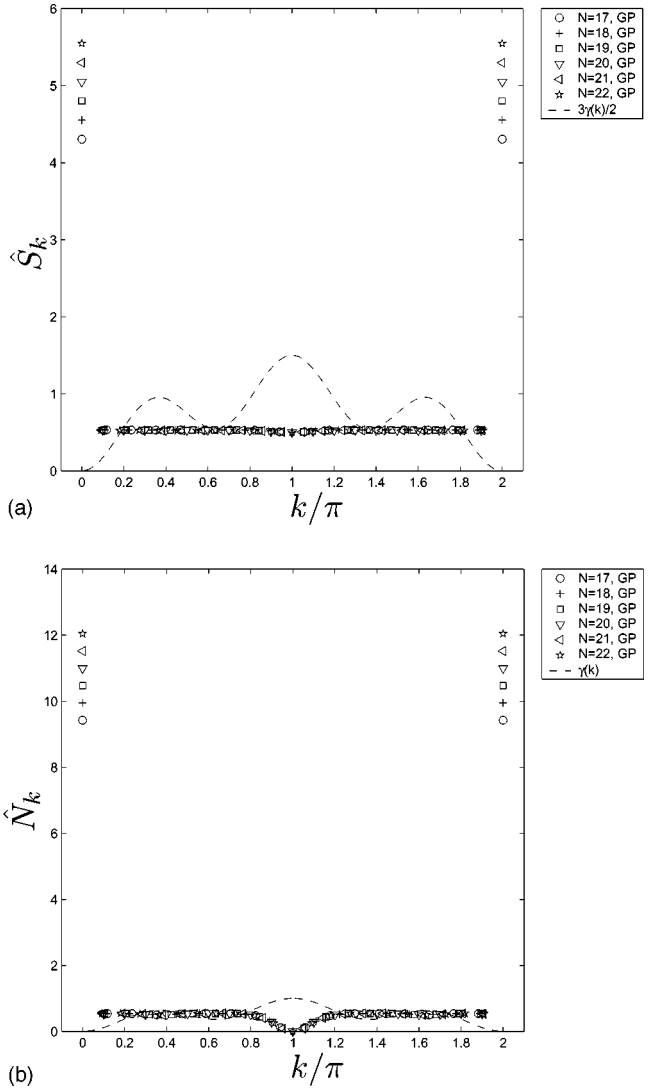

FIG. 4. High-spin Lanczos calculation on the $p=3$ spiral with periodic local boundary conditions and global boundary conditions indicated in the key (GA=globally antiperiodic, GP=globally periodic). (a) $\hat{S}_{\mathbf{k}}$ and (b) $\hat{N}_{\mathbf{k}}$. The dashed lines represent the structure factor for comparison.

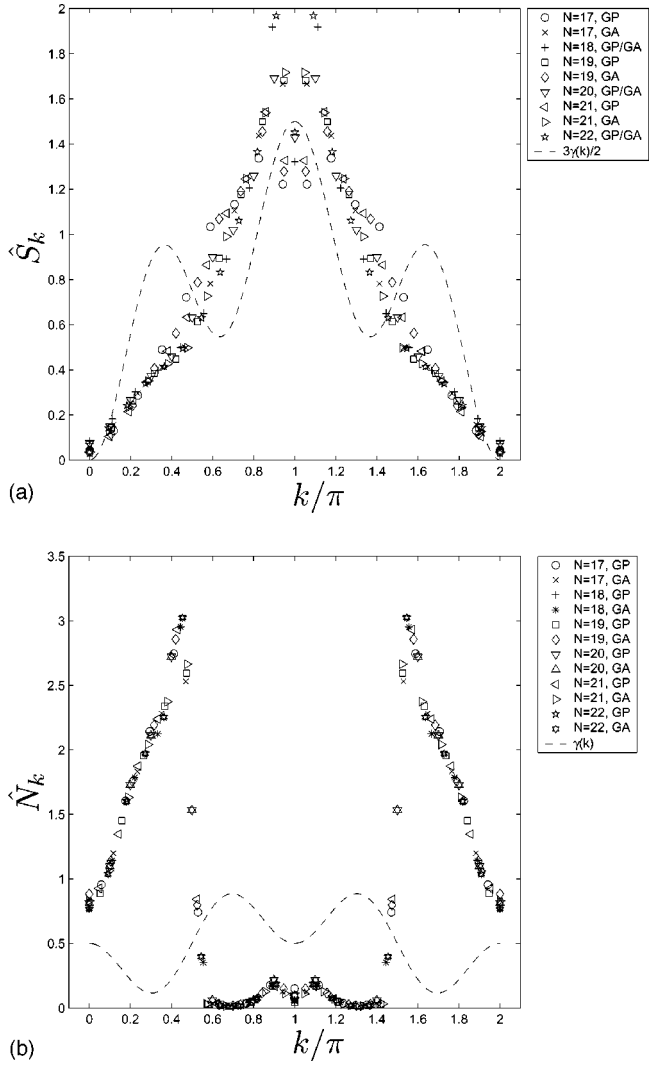

FIG. 5. Low-spin Lanczos calculation on the $p=3$ spiral with antiperiodic local boundary conditions and global boundary conditions indicated in the key (GA=globally antiperiodic, GP =globally periodic). (a) $\hat{S}_{\mathbf{k}}$ and (b) $\hat{N}_k$. The dashed lines represent the structure factor for comparison.

then this is indicative of a Fermi liquid, whereas an N^{α} divergence suggests Luttinger-liquid behavior. If the divergence is absent, then the correlations are short range only, and the system becomes very difficult to classify.

These comments are best illustrated with an example. In Fig. 4 we show the results of finite-size Lanczos calculations on the $p=3$ spiral, with the restriction of high total spin, meaning that all spins are parallel, with the exception of a single flipped spin (the ferromagnetic state is trivial).

Clear linear divergences can be seen in both $\hat{S}_{\mathbf{k}}$ and $\hat{N}_k$, indicating both long-range ferromagnetism *and* Fermi-liquid behavior. Finite-range correlations are revealed via convergence as the system size becomes greater than the correlation length. These results should be contrasted with the low-spin ground state (Fig. 5) where $S_z=0$ (for an even number of spins) or $S_z=\frac{1}{2}$ (for an odd number of spins). The two quantities can be seen to cleanly converge to a finite limit, indicating that the system lacks magnetic long-range order and is *not* a Fermi liquid.

Renormalization group arguments suggest that the number of fundamental styles of behavior that a system may exhibit are highly restricted. We have already discussed Fermi liquids versus non-Fermi liquids, but each of these has important subcategories, and it is crucial to be able to identify and distinguish between these distinct states. We have already discussed how to identify a Fermi liquid, but it may occur in two basic forms: single component and two component. The two component Fermi liquids are distorted noninteracting systems with the same symmetry and with spin degeneracy in the quasi particles. The single-component Fermi liquids tend to be magnetic, and the broken spin symmetry gives singly degenerate branches of quasiparticles. These distinct situations can be distinguished using the position of the divergence in the scaled occupation number. If it should occur at an extremum of the underlying structure fac-

tor, then there are pools of quasiparticles, and this is typical of a single-component fluid. If the divergence occurs at the noninteracting Fermi level, which tends to be at a point of inflection in the structure factor, then the system is a two-component fluid. To determine which type of fluid we may be dealing with, we must determine whether we have a large or small Fermi surface. In our calculations, we add a single oxygen hole and so the small Fermi surface corresponds to the single-component case and a small pool of electrons being generated at an extremum of the structure factor. The experimentally relevant large Fermi surface case involves the background copper spins contributing towards the Fermi surface and the two-component fluid picture. We find the second case in our calculations and offer a picture of how the single hole can dominate all the copper spins and push them towards this large Fermi surface picture.

Non-Fermi liquids are much more subtle as they are rather less well understood than Fermi liquids, but we can identify two broad subcategories. The best known are the Luttinger liquids, which we have already discussed briefly. Like the Fermi liquids, the Luttinger liquids also display a divergence in the scaled occupation number, but the divergence is not linear, varying as N^{α}, where $0<\alpha<1$. Both types of Fermi liquid can provide an analogous Luttinger liquid, but the magnetic order associated with the two-component fluid is generally expected to be prohibited. The second type of non-Fermi liquid is the least well understood and hence the most interesting: pure quantum states with no divergence of the occupation number. Such states have only short-range correlations, and typical examples are valence bond solids and so-called resonating valence bond (RVB) states. The correlation length can be significant, and these states are indistinguishable from the other types until the system size is larger than the correlation length, when the correlations are seen to converge to a finite limit. Such systems are distinguished by their correlation length, and it is important to be able to identify this.

In the following sections of this article, we will show that the model we propose for the high-T_c superconductors can indeed exhibit such a quantum ground state. Such states have been observed in other models, and there are exact solutions present in the literature. The most relevant is the t model on cage geometries.[22] In this model, a collection of atoms form a cage if each atom has chemical bonds of equal strength to every other atom in the cage. If there are n atoms in a cage and each atom is in p cages, then the Nagaoka problem may be solved exactly provided $n \geqslant 2p$. The solution is a resonating valence bond state, where the hole is delocalized over the space of valence bond states containing one valence bond in each cage. The hole delocalizes by hopping onto these valence bonds, generating an exponentially large superposition of such states. Some examples of such geometries are the pyrochlore lattice and the checkerboard square lattice with additional diagonal bonds on the black squares. The simplest example is a chain of edge-sharing tetrahedra (with double bonds on the connected edges) which offers some of the interesting phenomena exhibited by such systems, but not all. The solution of this simple case is a valence bond solid containing a mobile hole with an additional bound spinon and is quite easy to understand, providing a useful reference point for this work.

III. ANALYTICAL RESULTS

In this section we present a novel variational technique with which we are able to calculate the type of classical spin spiral preferred by the motion of a single hole on our spiral geometries. The technique is a generalization of standard spin-wave theory to the motion of a single hole: we assume that the hole motion will prefer a spin spiral and then add quantum fluctuations to determine the *spiral pitch* which optimizes the hole motion.

To begin, we make a classical ansatz for the spin state: each copper site is given a fixed quantization direction, and this direction spirals from site to site. Noting that the hole resides on a separate sublattice, we must also assign a quantization direction to the oxygen sites, and we choose this to be continuous with the copper lattice. The pitch of this spin spiral k^* is treated as a variational parameter over which we will optimize. In addition, the hole is allowed to delocalize with wave vector q^* which must also be optimized. For all the systems we have analyzed in this paper, we found that $q^*=0$ is the optimum, and there is no need to discuss this parameter any further.

It is useful to consider how this approach relates to standard spin-wave calculations. In the magnetic problem defined by the Heisenberg model, the pitch of the spin spiral is set by the classical limit. Semiclassical spin fluctuations then allow quantum effects to attempt to break down the classical state. In the current problem, we have no direct magnetic interaction and so the spiral pitch is not governed by the classical limit, but is determined at the semiclassical level, where the hole binds into a Zhang-Rice singlet, which then delocalizes. This is why we must treat the spiral pitch as a variational parameter over which to optimize.

It may seem strange to perform semiclassical variational calculations on a system which one would expect to be governed absolutely by quantum effects. The reason we consider these calculations to be useful is that they allow us to compare the numerical calculations discussed in Sec. IV with semiclassical predictions. In fact we will see that some of the numerical results show some semiclassical characteristics, and these calculations provide a useful consistency check. They are especially useful since they are not constrained by finite system size, and so finite-size effects in the numerical work may be identified.

The first step toward the variational calculations we wish to perform is to rerepresent the Hamiltonian in our chosen basis. We allow the spins to spiral in the xy plane and using the z axis for quantization, the vacuum state may be written as

$$|\phi\rangle = \frac{1}{\sqrt{2}}\left[e^{-i\phi/2}|\uparrow\rangle + e^{i\phi/2}|\downarrow\rangle\right], \tag{29}$$

which is a classical spiral with each spin canted at an angle ϕ relative to the x axis. Semiclassical fluctuations from this ground state are, as in classical spin-wave theory, described by Holstein-Primakoff bosons[23] which are written as

$$b^\dagger|\phi\rangle = \frac{\mathrm{i}}{\sqrt{2}}\left[-\mathrm{e}^{-\mathrm{i}\phi/2}|\uparrow\rangle + \mathrm{e}^{\mathrm{i}\phi/2}|\downarrow\rangle\right], \tag{30}$$

where the quantization direction on each site has been chosen to be parallel to the classical spin orientation. This leads to a complication when describing the motion of the boson. The direct hopping of the hole from site to site (via t) requires these states to be rerepresented using a different orientation. When the hole hops from a site with quantization direction ϕ to a site with quantization direction ϕ', it hops with an amplitude $\cos[(\phi-\phi')/2]$ without a spin fluctuation and simultaneously hops with an amplitude $\pm\sin[(\phi-\phi')/2]$ with a spin fluctuation. This provides

$$|\phi\rangle = \left[\cos\frac{\phi-\phi'}{2} + \sin\frac{\phi-\phi'}{2}b'^\dagger\right]|\phi'\rangle, \tag{31}$$

$$b^\dagger|\phi\rangle = \left[\cos\frac{\phi-\phi'}{2}b'^\dagger + \sin\frac{\phi-\phi'}{2}\right]|\phi'\rangle. \tag{32}$$

The X term is significantly more complicated as this also involves the copper spins. We denote the copper spin quantization directions using θ, and the angle ϕ must now be represented in terms of θ, which must in turn be represented in terms of ϕ'. We have

$$|\phi,\theta\rangle = \cos\frac{\phi-\theta}{2}\cos\frac{\theta-\phi'}{2}|\phi,\phi'\rangle + \cos\frac{\phi-\theta}{2}\sin\frac{\theta-\phi'}{2}b'^\dagger|\phi,\phi'\rangle + \sin\frac{\phi-\theta}{2}\cos\frac{\theta-\phi'}{2}a^\dagger|\theta,\phi'\rangle + \sin\frac{\phi-\theta}{2}\sin\frac{\theta-\phi'}{2}b'^\dagger a^\dagger|\theta,\phi'\rangle, \tag{33a}$$

$$b^\dagger|\phi,\theta\rangle = \cos\frac{\phi-\theta}{2}\cos\frac{\theta-\phi'}{2}a^\dagger|\theta,\phi'\rangle + \cos\frac{\phi-\theta}{2}\sin\frac{\theta-\phi'}{2}a^\dagger b'^\dagger|\theta,\phi'\rangle - \sin\frac{\phi-\theta}{2}\cos\frac{\theta-\phi'}{2}a^\dagger|\theta,\phi'\rangle - \sin\frac{\phi-\theta}{2}\sin\frac{\theta-\phi'}{2}b'^\dagger|\theta,\phi'\rangle, \tag{33b}$$

$$a^\dagger|\phi,\theta\rangle = \cos\frac{\phi-\theta}{2}\cos\frac{\theta-\phi'}{2}b'^\dagger|\theta,\phi'\rangle + \cos\frac{\phi-\theta}{2}\sin\frac{\theta-\phi'}{2}|\theta,\phi'\rangle + \sin\frac{\phi-\theta}{2}\cos\frac{\theta-\phi'}{2}b'^\dagger a^\dagger|\theta,\phi'\rangle - \sin\frac{\phi-\theta}{2}\sin\frac{\theta-\phi'}{2}a^\dagger|\theta,\phi'\rangle, \tag{33c}$$

$$a^\dagger b^\dagger|\phi,\theta\rangle = \cos\frac{\phi-\theta}{2}\cos\frac{\theta-\phi'}{2}a^\dagger b'^\dagger|\theta,\phi'\rangle + \cos\frac{\phi-\theta}{2}\sin\frac{\theta-\phi'}{2}a^\dagger|\theta,\phi'\rangle - \sin\frac{\phi-\theta}{2}\cos\frac{\theta-\phi'}{2}b'^\dagger|\theta,\phi'\rangle + \sin\frac{\phi-\theta}{2}\sin\frac{\theta-\phi'}{2}|\theta,\phi'\rangle, \tag{33d}$$

where $a^\dagger$ creates a fluctuation on the intermediate copper site. The motion now involves up to two fluctuations per hop and is clearly quite complex.

These results now allow us to construct a second-quantized description of the hole moving in our classical spin spiral under the action of the t-X Hamiltonian. We use an operator $h_j^\dagger$ to create a hole at oxygen site j, and a *single* boson $b^\dagger$ to denote any fluctuation of the *hole's* spin. An array of bosons $a_i^\dagger$ describes copper spin fluctuations, and our vacuum state $|0\rangle$ corresponds to the state with all spins oriented parallel to their classical quantization directions. We can hence represent the direct hole hopping as

$$\mathcal{H}_t = -t\sum_{\langle ij\rangle}\sum_{\langle ij'\rangle} h_{j'}^\dagger h_j\left[\cos\frac{\phi_j-\phi_{j'}}{2} + \sin\frac{\phi_j-\phi_{j'}}{2}(b^\dagger - b)\right], \tag{34}$$

and the more important "shuffling" interaction can similarly be written as

$$\mathcal{H}_X = X\sum_{\langle ij\rangle}\sum_{\langle ij'\rangle} h_{j'}^{\dagger}h_j\Bigg(\cos\frac{\phi_j-\theta_i}{2}\cos\frac{\theta_i-\phi_{j'}}{2}[a_ia_i^{\dagger}bb^{\dagger}+a_i^{\dagger}a_ib^{\dagger}b+a_i^{\dagger}b+a_ib^{\dagger}]$$
$$+\sin\frac{\phi_j-\theta_i}{2}\sin\frac{\theta_i-\phi_{j'}}{2}[a_i^{\dagger}b^{\dagger}+a_ib-a_i^{\dagger}a_ibb^{\dagger}-a_ia_i^{\dagger}b^{\dagger}b]+\cos\frac{\phi_j-\theta_i}{2}\sin\frac{\theta_i-\phi_{j'}}{2}[a_ia_i^{\dagger}b^{\dagger}+a_i^{\dagger}b^{\dagger}b+a_ibb^{\dagger}+a_i^{\dagger}a_ib]$$
$$+\sin\frac{\phi_j-\theta_i}{2}\cos\frac{\theta_i-\phi_{j'}}{2}[a_i^{\dagger}bb^{\dagger}+a_i^{\dagger}a_ib-a_ia_i^{\dagger}b-a_ib^{\dagger}b]\Bigg) \tag{35}$$

or, in a more physically instructive form,

$$\mathcal{H}_X = \frac{X}{2}\sum_{\langle ij\rangle}\sum_{\langle ij'\rangle} h_{j'}^{\dagger}h_j\Bigg(\cos\frac{\phi_i-\phi_{j'}}{2}[1-(a_i^{\dagger}-a_i)(b^{\dagger}-b)]+\cos\Bigg(\theta_i-\frac{\phi_i+\phi_{j'}}{2}\Bigg)[(a_ia_i^{\dagger}-a_i^{\dagger}a_i)(bb^{\dagger}-b^{\dagger}b)+(a_i^{\dagger}+a_i)(b^{\dagger}+b)]$$
$$+\sin\frac{\phi_i-\phi_{j'}}{2}[a_i^{\dagger}-a_i+b^{\dagger}-b]+\sin\Bigg(\theta_i-\frac{\phi_i+\phi_{j'}}{2}\Bigg)[(a_ia_i^{\dagger}-a_i^{\dagger}a_i)(b^{\dagger}+b)-(a_i^{\dagger}+a_i)(bb^{\dagger}-b^{\dagger}b)]\Bigg). \tag{36}$$

These representations are *exact* and can be used to reproduce the exact solutions discussed earlier. For the simple case of a pure ferromagnet, all the angles are equal, and at $t=X$, the model reduces to

$$\mathcal{H} = t\sum_{\langle ij\rangle}\sum_{\langle ij'\rangle} h_{j'}^{\dagger}h_j[a_i^{\dagger}b+a_ib^{\dagger}-a_ia_i^{\dagger}b^{\dagger}b-a_i^{\dagger}a_ibb^{\dagger}] \tag{37}$$

and hence

$$\mathcal{H}h_l^{\dagger}(b^{\dagger}-a_i^{\dagger})|0\rangle = -2t\sum_{\langle ij\rangle} h_{j'}^{\dagger}(b^{\dagger}-a_i^{\dagger})|0\rangle$$
$$-t\sum_{\langle i'j'\rangle} h_{j'}^{\dagger}(b^{\dagger}-a_{i'}^{\dagger})|0\rangle, \tag{38}$$

where ili' are a set of three neighboring atoms—viz., Cu-O-Cu—and the oxygen sites j and j' are the neighbors of copper sites i and i' (note that $j=l$ and $j'=l$ are both allowed). This is in complete agreement with the exact solution at this point in parameter space. This representation allows a completely free choice of classical spin background, constrained only by the restriction to planar spins. However, for our choice of geometry there are additional constraints. For the simplest geometry, the linear chain, we have

$$\theta_i = \frac{\phi_j+\phi_{j'}}{2}, \tag{39}$$

and this situation is much simpler. There are also cases where the hole does not move and simply exchanges its spin with the neighboring copper site. In this case, $\phi_j=\phi_{j'}$, another simplification.

Unlike semiclassical spin-wave theory, where we describe coherent fluctuations perpendicular to the classical spin orientations, in this problem we are trying to describe a spin *polaron*. The hole induces local spin correlations which optimize its motion. One possibility which we may expect from the exact solutions is that the hole will bind in a Zhang-Rice singlet, and as the hole moves around, longer-range spin correlations must also be generated to ensure that it remains in a local singlet. In turn, this maximizes its motion around the many closed loops in our chosen geometries. It has been suggested that the hole carries a local "spin deformation" (a polaron) with it, but in fact the hole can only interact with copper spins on sites which it travels across, and so as the hole moves, it generates new spin correlations between the sites it traverses, leaving a "trail" of correlations. These diminish at greater distances from the hole, fading into a preferred "background state." In these calculations, we assume that the background state is a pure spin spiral and we need to incorporate the local fluctuations that optimize the hole motion. Since the preferred background is *not* likely to be a pure spiral, the hole will also attempt to generate longer-range fluctuations of the preferred order.

In these calculations, we begin with the classical spiral state. We then generate all states connected to this state via iterative applications of the Hamiltonian. This amounts to successively "hopping" the hole and so the induced spin fluctuations must be close to the hole, being within the number of hops applied so far. The size of the state space increases exponentially and we have to diagonalize large Hamiltonian matrices, but this can be done for a size up to about $200\,000\times200\,000$. The resultant energies are a function of spiral pitch, and the spiral pitch which optimizes the motion can easily be found. In this sense, the calculations are truly variational. In Fig. 6 we show the results of such a calculation on the linear chain at $t/X=0$.

This problem has been previously studied[24] and is known to have a locally distorted Heisenberg ground state, in which the hole acts like a spinon. The ground-state energy is below $-2.895X$, and our calculations obtain about 99% of this energy. The optimal pitch k^* appears to be converging on the antiferromagnetic point. It should be noted that this is a particularly difficult example to interpret as the hole carries a spinon and hence there is a domain wall in the system which is very difficult to approximate within our spiral ansatz. The result is a compromise in which the optimal pitch is kept away from the antiferromagnetic point to allow the spins neighboring the hole to be partially parallel, as is required by the true solution.

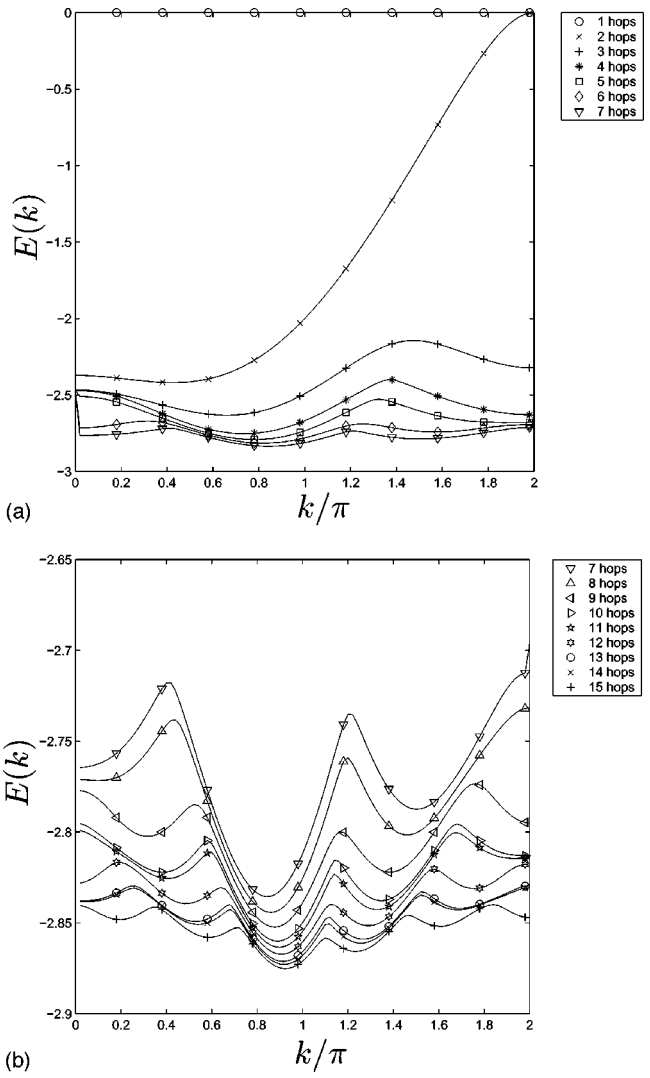

FIG. 6. Classical spin spiral energies on the linear chain at $t/X=0$, as a function of spiral pitch. These graphs show the effect of adding progressively more hops. (a) 1–7 hops included and (b) 7–15 hops included.

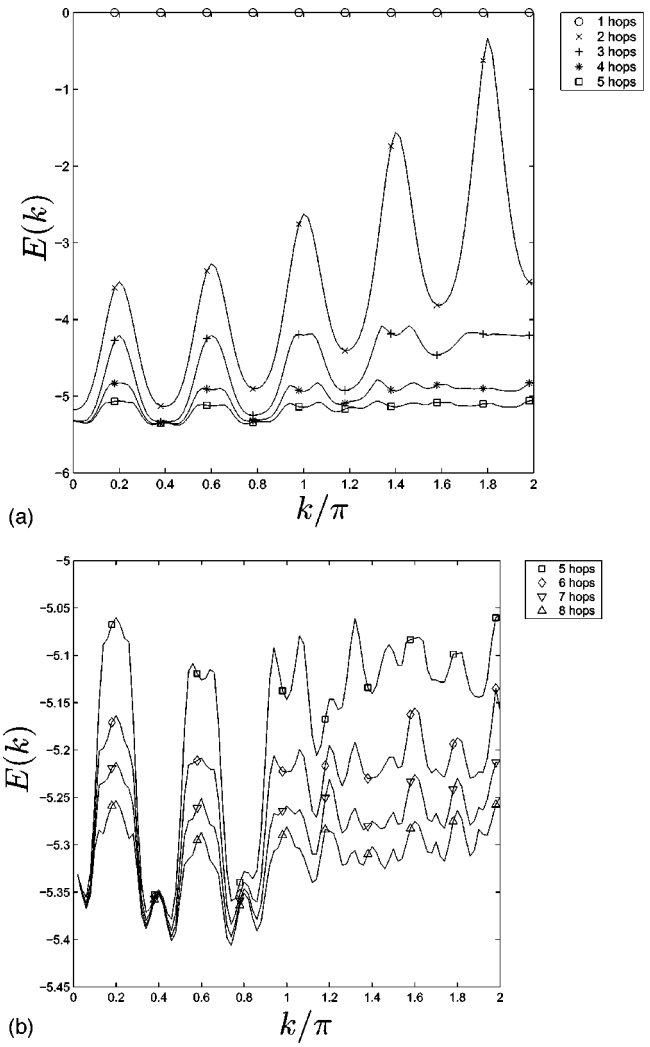

FIG. 7. Classical spin spiral energies on the $p=11$ spiral at $t/X=0$, as a function of spiral pitch. These graphs show the effect of adding progressively more hops. (a) 1–5 hops included and (b) 5–8 hops included.

The nature of domain walls in two dimensions, where the domain wall is a one-dimensional object and cannot be treated as a pointlike excitation, means that two-dimensional systems are more subtle. In Fig. 7 we show the classical spiral energies for $p=11$. This system contains a fairly long-range hop, and we might expect it to demonstrate some two-dimensional character. Much less variation is seen in the optimum spiral pitch than was seen in the linear chain. Also note that the zero-pitch spiral corresponding to ferromagnetism is *unstable*, and the ground state to the X model on this geometry is very nontrivial.

Once the optimal pitch has been found, one can find the associated sequence of ground states and determine a sequence of approximations to the desired correlation functions. Including more extensive hops in the calculations is analogous to finite-size scaling, but note well that this type of calculation does not describe the magnetism very well. There are always a macroscopic number of spins which have not yet been affected by the longest hops, and these will always dominate over the fluctuations which are solely within the range of the longest hop. The resulting magnetism is dominated by classical behavior. However, this technique is a useful probe of the occupation number that we might expect this model to provide, since the background spins do not contribute directly, and the correlations are dominated by the fluctuations in the vicinity of the hole. As we discussed previously there are two types of behavior which are superimposed: smooth short-range correlations and divergent peaks. The short-range correlations are indicative of local quantum fluctuations which serve to optimize the hole's motion locally, while the divergent peaks indicate Fermi- and Luttinger-liquid-like behavior. Since these calculations are performed on infinite systems, true δ-function peaks can and do occur. However, the underlying classical spin background adds a complication. The induced fluctuations are necessarily near to the hole, and the underlying classical spiral controls the behavior outside of this region. The finite probability that the state is exactly the pure classical spiral provides the δ-function contribution to begin with (when there are no

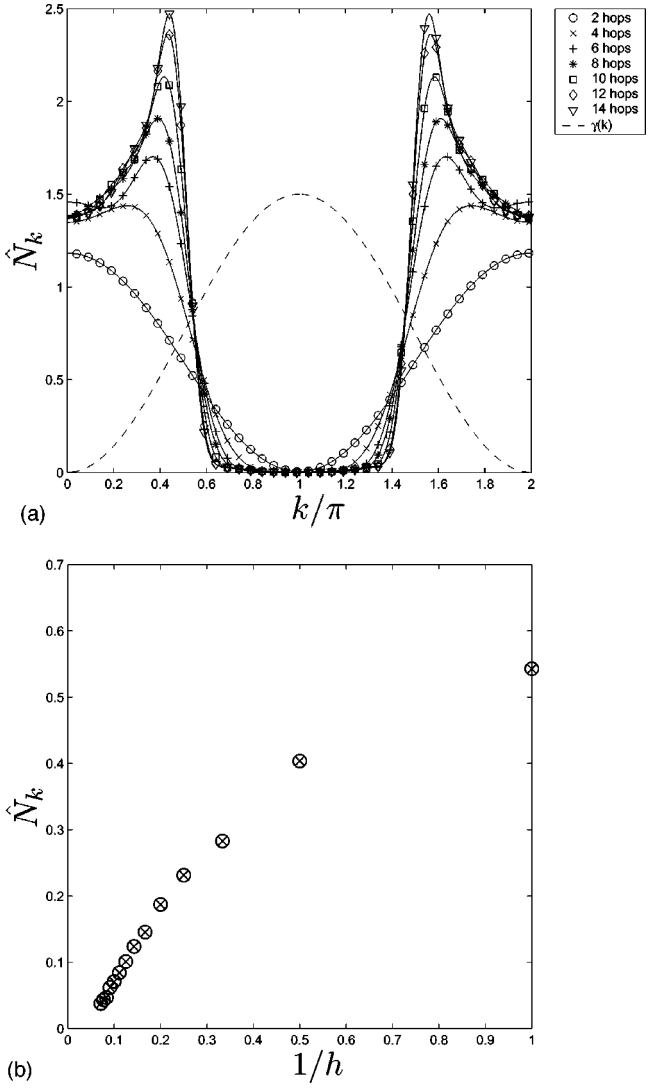

FIG. 8. $\hat{N}_k$ calculated on the linear chain. (a) Overlay of short-range contributions for number of hops, $0 \leqslant n \leqslant 11$. (b) Magnitude of the long-range component plotted against $1/h$, where h is the number of hops included in the calculation. The dashed line represents the underlying structure factor. For labeling purposes, symbols are provided at only a few data points, and the lines pass through all data points.

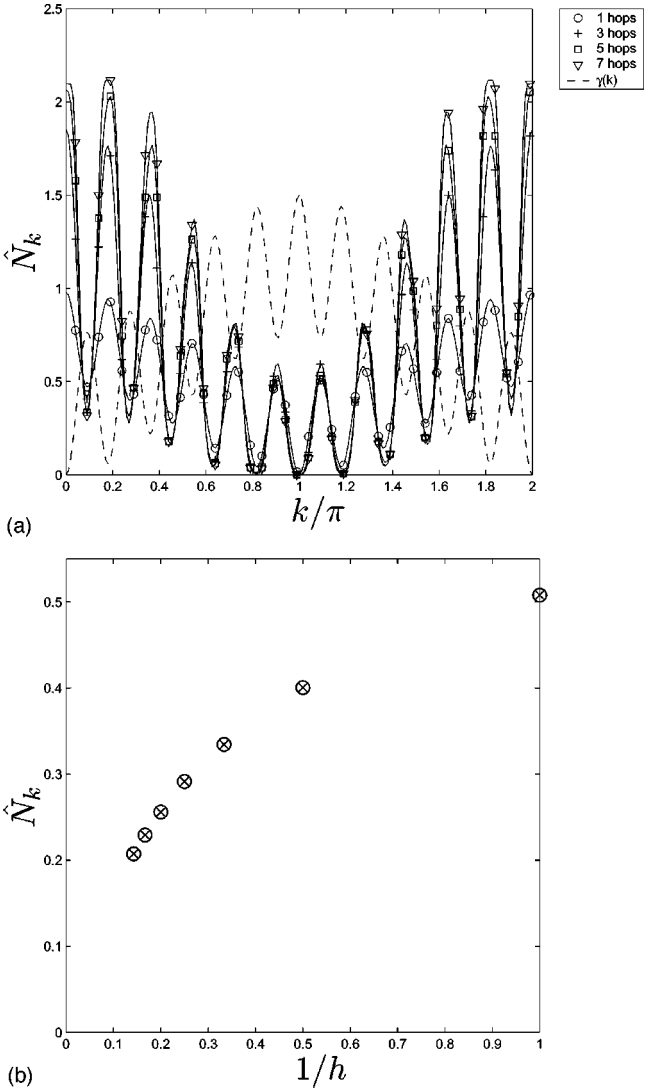

FIG. 9. $\hat{N}_k$ calculated on the $p=11$ spiral with antiperiodic local boundary conditions. (a) Overlay of short-range contributions for number of hops, $0 \leqslant n \leqslant 11$. (b) Magnitude of the long-range plotted against $1/h$, where h is the number of hops included in the calculation. The dashed line represents the underlying structure factor.

fluctuations). As hops are added to the calculation, the probability of the state being the pure spiral decreases and hence so does the weight of the δ function. If the system is a pure Fermi liquid, then the weight from the δ function is transferred into a divergent peak in the short-range contribution, which provides the long-range character (rather than the classical spiral).

Due to the difficulties involved in performing calculations involving long-range hops, we are restricted to study relatively small numbers of fluctuations. We expect a robust δ-function contribution to be a good indication of a divergence, but eventually it must vanish, due to the preceding argument. In order to circumvent this difficulty, we choose to calculate and extract the long-range behavior and the pure short-range correlations separately. The results for the linear chain are given in Fig. 8.

It is clear from Fig. 8(b) that the long-range component is decaying to zero as the calculations become more sophisticated, and this system is, as expected, not a Fermi liquid. The form of $\hat{N}_k$ shown in Fig. 8(a) is highly instructive and should be analyzed carefully. The system mirrors the half-filled noninteracting Fermi liquid state, with the *localized* spins acting as the half-filled Fermi sea. For a noninteracting solution we expect

$$|\psi\rangle = \prod_{k \in \mathcal{K}, \sigma} [\cos \theta_k d^\dagger_{k\sigma} + \sin \theta_k p^\dagger_{k\sigma}]|0\rangle, \tag{40}$$

where $\mathcal{K}$ is the set of all filled states. In the limit that the copper states are much preferred, $\theta_k \ll 1$, and we expect a small admixture of oxygen holes in the occupied region. This describes the short-range contribution to $\hat{N}_k$ very well. When we *add* a fermion to our noninteracting state, the *change* in

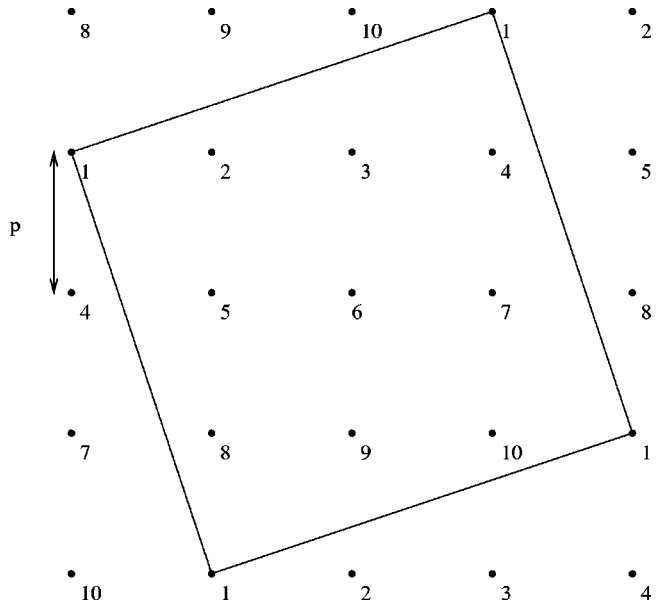

FIG. 10. An example ($p=3$, $N=10$) of how the spiral systems correspond to the square lattice. The numbering represents the ordering of the sites on the backbone of the spiral.

$\hat{N}_k$ is localized at the Fermi surface, and the next available state is occupied, extending the Fermi surface slightly. This provides an excellent description for the divergence in $\hat{N}_k$.

In fact, this system is *not* a Fermi liquid, and $\hat{N}_k$ at the Fermi surface diverges with a power law. Note, however, that our limiting procedure is not smooth since the preferred spiral pitch slowly migrates toward the antiferromagnetic point (but not closer than 10% in our calculations). The position of the discontinuity does not agree with the pitch of the spiral, but is exactly one-half of the pitch, in agreement with the result that magnetism in Fermi liquids arises from nesting between the two Fermi points, giving $q=2k_F$.

The spiral systems we wish to study are much more complex than the linear chain. The finite spiral corresponds in reciprocal space to a sequence of parallel lines which cross the Brillouin zone p times. A two-dimensional peak is seen as a series of one-dimensional peaks which rise and fall as the parallel lines cross the peak in different places (Fig. 3). The correlations for the system with $p=11$ are shown in Fig. 9.

A sequence of p peaks can be seen in Fig. 9(a) at the p places where the the reciprocal-space lattice crosses the two-dimensional Brillouin zone. The peaks are clearly found in the minima of the underlying structure factor as expected, but there is no longer a clear distinction between structured regions and the (vanishing) gaps between them.

The long-range component does not occur at these peaks, but is at the position of maximum slope, in keeping with the Fermi-liquid picture. The convergence of the long-range contribution is not clear, and one cannot confidently predict Fermi-liquid behavior or otherwise from these results, although it should be noted that the long-range contribution is converging [Fig. 9(b)] much more slowly than was the case for the linear chain [Fig. 8(b)]. It is also very instructive to note that as the δ function decays, its weight is not simply

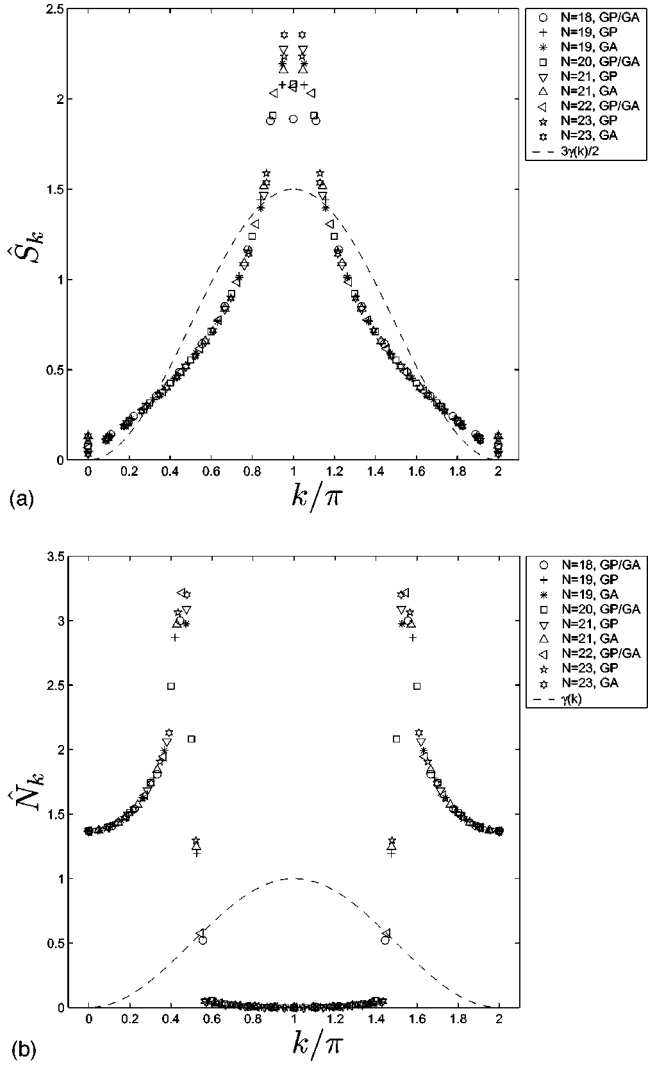

FIG. 11. Finite-size-scaled correlation functions for a single hole on the CuO linear chain at $t/X=0$, with boundary conditions indicated in the key (GA=globally antiperiodic, GP=globally periodic). (a) $\hat{S}_k$ and (b) $\hat{N}_k$.

transferred to a corresponding peak in the short-range component, but is distributed fairly uniformly across all the maxima, suggesting an eventual result which is smooth and may correspond to a quantum solution.

The obvious difficulties in interpreting the results of these calculations mean that we are restricted to analyzing simple systems (small values of p) where convergence is most likely. This technique can be used to analyze these systems, but we can also use finite-size scaling of exact diagonalization calculations, which do not require a classical ansatz and can identify pure quantum behavior. These calculations are introduced in the next section.

IV. NUMERICAL CALCULATIONS

In this section we use the Lanczos algorithm to exactly solve some finite spiral systems. Computational limitations dictate that we are restricted to a number of sites, $N \leqslant 24$, and

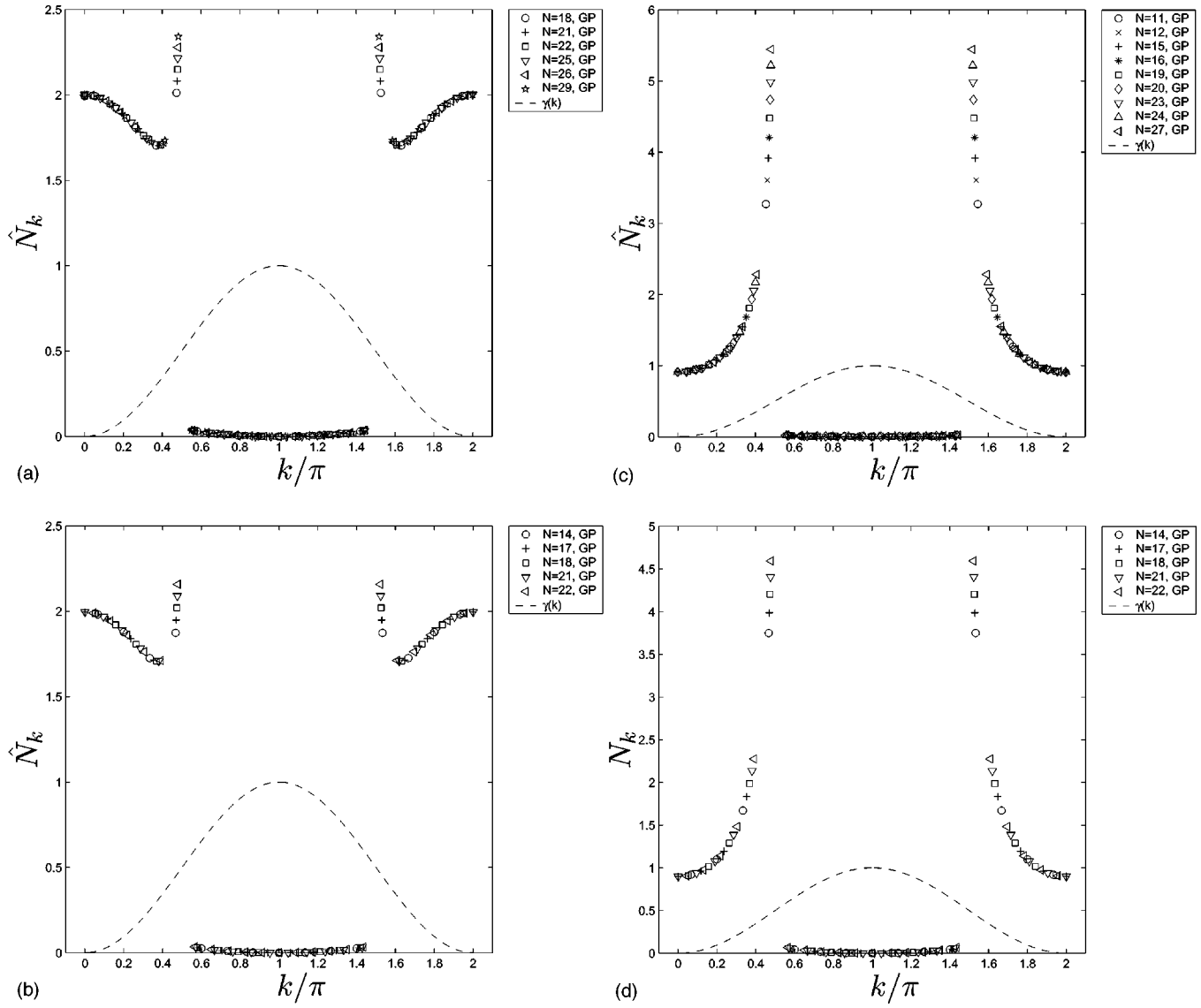

FIG. 12. A comparison of the occupation number correlations $N\hat{N}_k$ of the Heisenberg model with the predictions of the *t-X* model. (a) Heisenberg model plus Zhang-Rice singlet. (b) *t-X* model, $t=0.99X$. (c) Pure Heisenberg model. (d) *t-X* model, $t=-0.99X$. The dashed lines represent the underlying structure factor.

in turn, this limits our ability to study large values of p, the spiral pitch. The spiral systems correspond to the pure square lattice of interest when $N=p^2+1$ (as shown in Fig. 10), and so we can only study $1\leqslant p\leqslant 4$ completely. However, we can reach sufficiently large N to allow us to gain much insight into $p=5$ as well, although we cannot study the square system itself.

We begin our analysis with a study of the CuO linear chain. This system is quite well understood,[24] and it is useful to study this system as a reference point for forthcoming calculations. Since this system does not belong to our class of spiral systems, there are only global boundary conditions, and this makes interpretation of the results considerably simpler. The spin and number correlations for this system at $t/X=0$ are shown in Fig. 11.

It has been shown[24] that in this system, the hole acts as a spinon which stabilizes the ground state of the Heisenberg model as the ground state of this model as well. This is confirmed by the weak logarithmic divergence with respect to system size seen in Fig. 11(a), which is the closest to long-range order that the Heisenberg interaction can generate in one-dimensional (1D) systems. The spinon formed by the hole has the effect of pushing weight away from $k=\pi$ to the neighboring k points, reducing the divergence somewhat. The occupation number is completely consistent with that obtained by the semiclassical spiral calculations of Sec. III: the short-range contribution is very well converged, and the long-range contribution diverges with a power law with exponent $\alpha\approx 0.375$, consistent with the Luttinger liquid that one would expect in 1D. For comparison, it has been shown[24] that for the pure Heisenberg model, $\alpha=0.5$. Note that due to the finite number of points in k space, it is very hard to calculate this exponent exactly.

In Sec. I, we developed two exact solutions of the *t-X* model which we can analyze in more detail on the linear chain geometry. Recall there are two solutions, at $t=\pm X$,

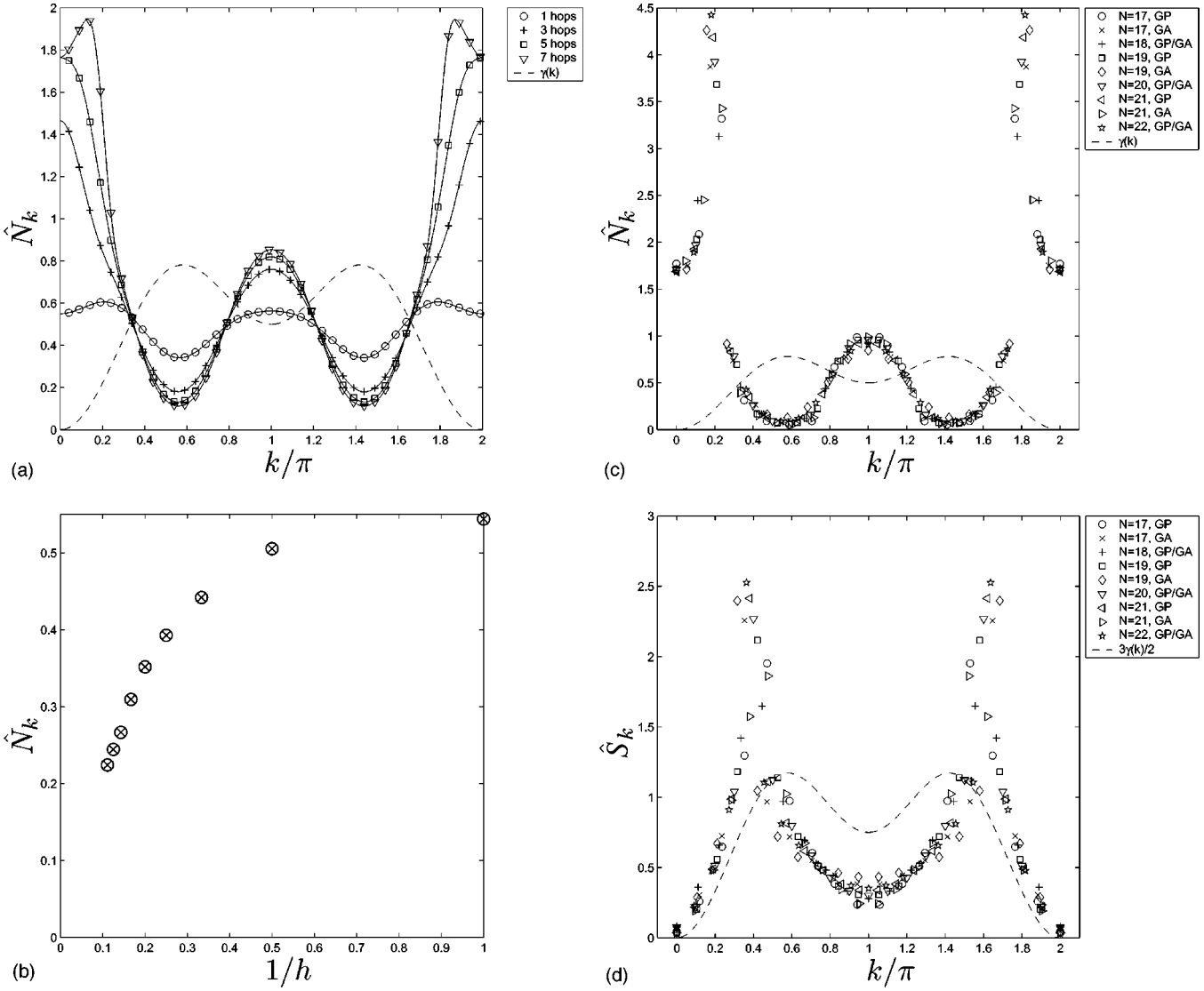

FIG. 13. Correlations on the $p=2$ spiral with periodic local boundary conditions, from (a), (b) semiclassical spiral calculation; (c), (d) finite-size scaled Lanczos calculations. (a) Short-range contribution to $\hat{N}_k$. (b) Long-range contribution to $\hat{N}_k$. (c) Finite-size scaled $\hat{N}_k$. (d) Finite-size scaled $\hat{S}_k$.

where the hole is decoupled from the copper spins, and there is huge spin degeneracy at these points, rendering a numerical solution impossible. We can, however, solve the model very close to the limits, and we will consider the points $t=\pm 0.99X$.

Consider first the point $t=X$. In this limit we have already determined that the model reduces to the hopping of a Zhang-Rice singlet on the copper lattice. For the two-dimensional square lattice, this motion stabilizes ferromagnetism,[20] but in one dimension it does not permute the spins, leaving all spin configurations degenerate. If we move away from $t=X$ to $t=0.99X$, then this introduces a triplet-projector interaction [Eq. (8)] which lifts the degeneracy. The nicest intuitive picture one can provide for this is of a local eigenstate involving three spins, where two copper spins in a singlet become a Zhang-Rice singlet as explained in Sec. I. These interactions act as an effective Heisenberg interaction and stabilize the Heisenberg ground state for the background spins. An analysis of the motion of the hole in such a state reveals that one would expect the occupancy to be

$$N\hat{N}_k = \frac{(1+\cos k)}{3}\left[2 + 2\cos k + 2\sum_{n=1}^{\infty}\hat{R}_n \cos(n+1)k\right], \tag{41}$$

where the $\hat{R}_n$ are the cyclic permutation correlations of the Heisenberg model, given by

$$\hat{R}_n = \left\langle \prod_{m=1}^{n}\left[\frac{1}{2} + 2\hat{\mathbf{S}}_m \cdot \hat{\mathbf{S}}_{m+1}\right]\right\rangle, \tag{42}$$

which have previously been investigated.[25] This result is in agreement with the exact solution at $t=X$ discussed in Sec. I.

In the other limit $t=-X$, the degeneracy is larger and is lifted by the inclusion of a small amount of singlet projector

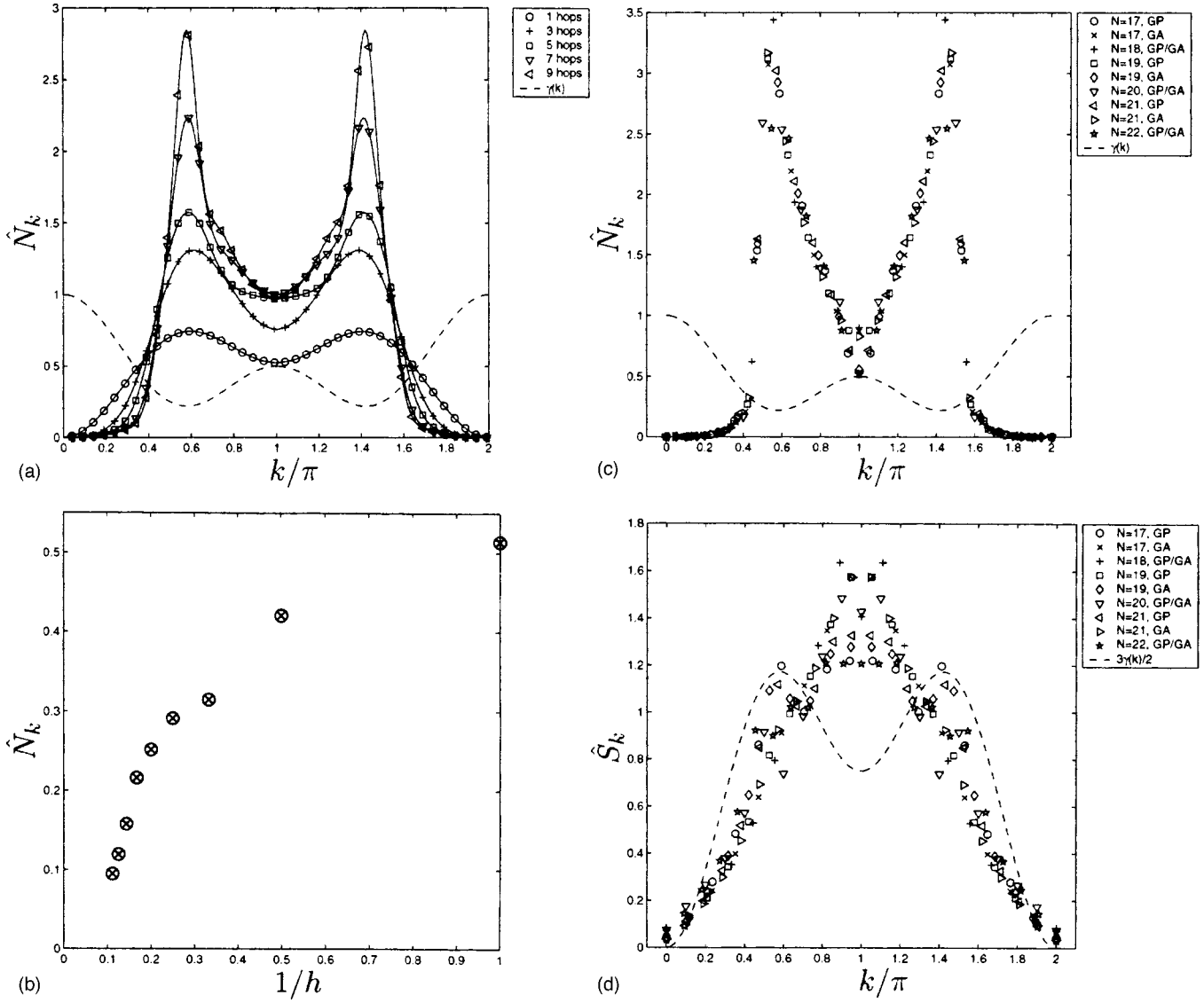

FIG. 14. Correlations on the $p=2$ spiral with antiperiodic local boundary conditions, from (a), (b) semiclassical spiral calculation; (c), (d) finite-size scaled Lanczos calculations. (a) Short-range contribution to $\hat{N}_k$. (b) Long-range contribution to $\hat{N}_k$. (c) Finite-size scaled $\hat{N}_k$. (d) Finite-size scaled $\hat{S}_k$.

interaction. The preferred state is then that of Eq. (20), where the order of the spins (including the oxygen hole) is preserved, and the singlet interaction stabilizes the Heisenberg ground state. The correlations in this case are predicted to be

$$N\hat{N}_k = 1 + 2\sum_{n=1}^{\infty} \hat{R}_n \cos nk. \tag{43}$$

The results of these calculations are shown in Fig. 12.

The Heisenberg model was solved numerically, and the cyclic permutation correlations $\hat{R}_n$ were calculated and inserted into Eqs. (41) and (43) to give graphs 12(a) and 12(c), respectively. The agreement with the numerical solutions of the *t-X* model [Figs. 12(b) and 12(d)] near the exact solutions is very good. Our assumption that the interaction of the hole with the spin background induces an effective Heisenberg spin interaction between neighboring spins in the background appears to be correct. We also note that our previous solution at $t/X=0$ is clearly in the same class as $t=-X$, with only a small contribution from the Zhang-Rice singlet, resulting in an increase in weight of the correlations at the zone center and a somewhat reduced peak at the zone boundary.

As we have already discussed, the divergence of the peak in $\hat{N}_k$ with system size as N^{α} indicates that a Luttinger-liquid phase is stabilized in the region $t<X$. This phase has all the properties expected of the *t-J* model in one dimension, but the physical origin of the spin correlations is very different, being due solely to the hole motion and *not* to the second-order Heisenberg interaction which is required to lift the spin degeneracy in the *t-J* model and which we have not included here. The physical interaction which stabilizes this low-spin state is therefore clearly missing from the *t-J* model. The nature of this interaction will become clear in the study of the spiral systems in the next section.

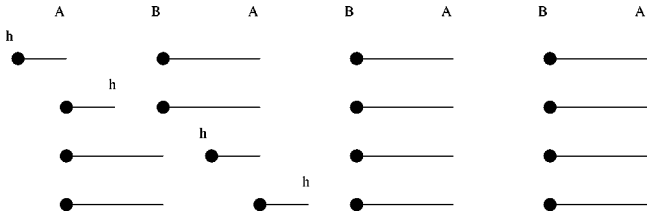

FIG. 15. The action of the Hamiltonian on a dimerized ground state leads to the hole becoming preferentially bound to one sublattice.

V. MAIN RESULTS

In the preceding sections we have introduced the basic techniques which we will use to study our sequences of spiral systems. It is very important that we retain complete control over these calculations, and hence we restrict ourselves to the understandable tight spiral systems ($2 \leqslant p \leqslant 5$), which we will study in order.

A. $p=2$ spiral

The $p=2$ spiral is the simplest system we will study in this section and contains bonds (via an oxygen site) to both nearest- and second-nearest-neighbor copper sites. The underlying copper lattice is hence essentially triangular, and one would expect this system to be frustrated in the conventional Hubbard model picture. Unlike our example calculation on the linear chain in the previous sections, we must consider both local and global boundary conditions in this calculation. We will be especially interested in the effect of the local boundary conditions, which one might presume to have a strong effect on the nature of the ground state stabilized. Periodic local boundary conditions correspond to an unfrustrated phase around one loop of the spiral which one would expect to stabilize high-spin correlations, while antiperiodic boundary conditions correspond to the frustrated phase which prefers low-spin correlations. This picture is somewhat oversimplified though, as the model itself is intrinsically frustrated and changes this picture somewhat as we shall see.

The results of both variational and numerical calculations are shown in Fig. 13.

The ground state has low spin and does not display any of the characteristics of the associated Hubbard model. The numerical calculation of $\hat{S}_k$ suggests that the system is susceptible to forming spin spirals with pitch $k^* \approx 2\pi/5$, in very good agreement with the semiclassical fluctuation calculations. The magnetic correlations are much stronger than in the linear chain, but do not converge in our numerical calculations as they extend beyond the size of our largest system.

The occupation number calculated numerically [Fig. 13(c)] is also clearly unconverged, but is nonetheless useful. The structure factor suggests *four* Fermi points at half-filling, located at

$$k_{\pm} = \pi - \arccos\left(\frac{1}{2\sqrt{2}}\right) \pm \frac{\pi}{4} = \pi(1 \pm 0.365), \pi(1 \pm 0.865), \tag{44}$$

with the pair closest to the zone center giving rise to the strong peaks which bound a strongly hybridized, but quite small region of filled Fermi sea, and the outer pair demarking a second region of more weakly hybridizing Fermi sea. The peaks are much stronger than in the linear chain, but careful analysis suggests that they are *not* divergent. The small occupied region is clearly smaller than the Fermi-gas solution might suggest, but the larger region is enhanced. This appears (to within the approximations enforced by the discrete nature of the system) to maintain the volume of the occupied region as expected from Luttinger's theorem.[26]

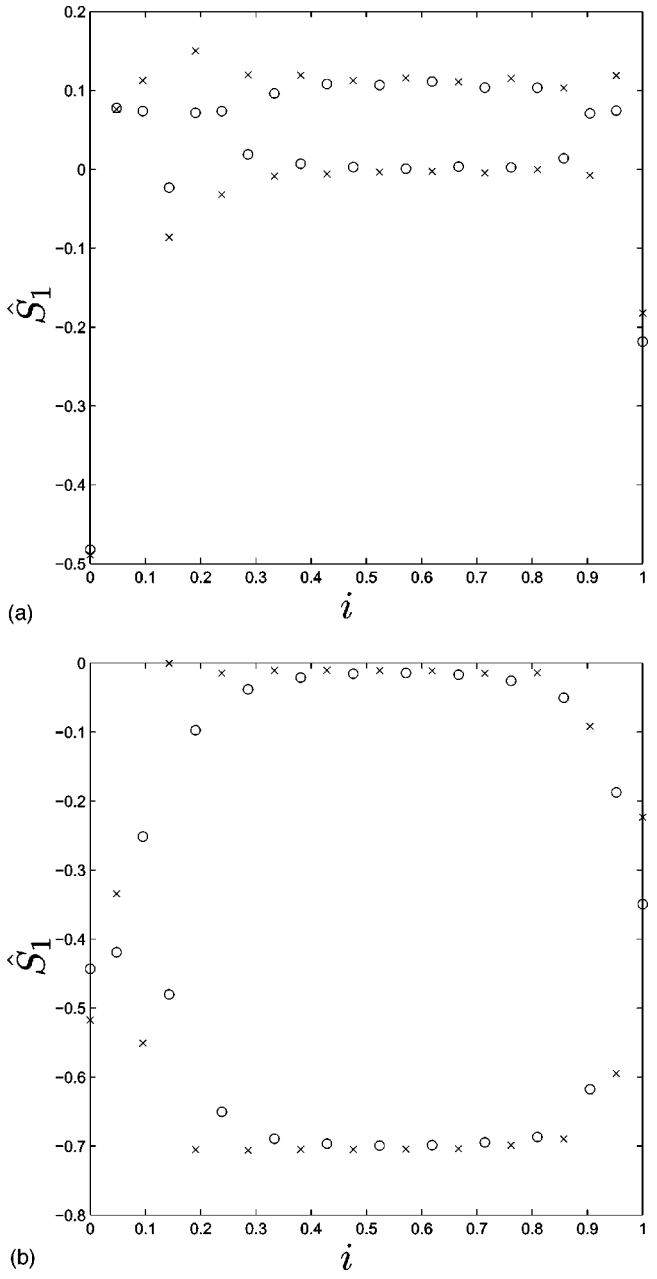

FIG. 16. Nearest-neighbor spin correlations as a function of position on the chain for (a) locally periodic and (b) locally antiperiodic boundary conditions on the $p=2$ spiral. The two ground states $|\phi_A\rangle$ and $|\phi_B\rangle$ are represented by the symbols $\times$ and $\bigcirc$, respectively.

For locally antiperiodic boundary conditions, the results are shown in Fig. 14. Both the spin correlations and number

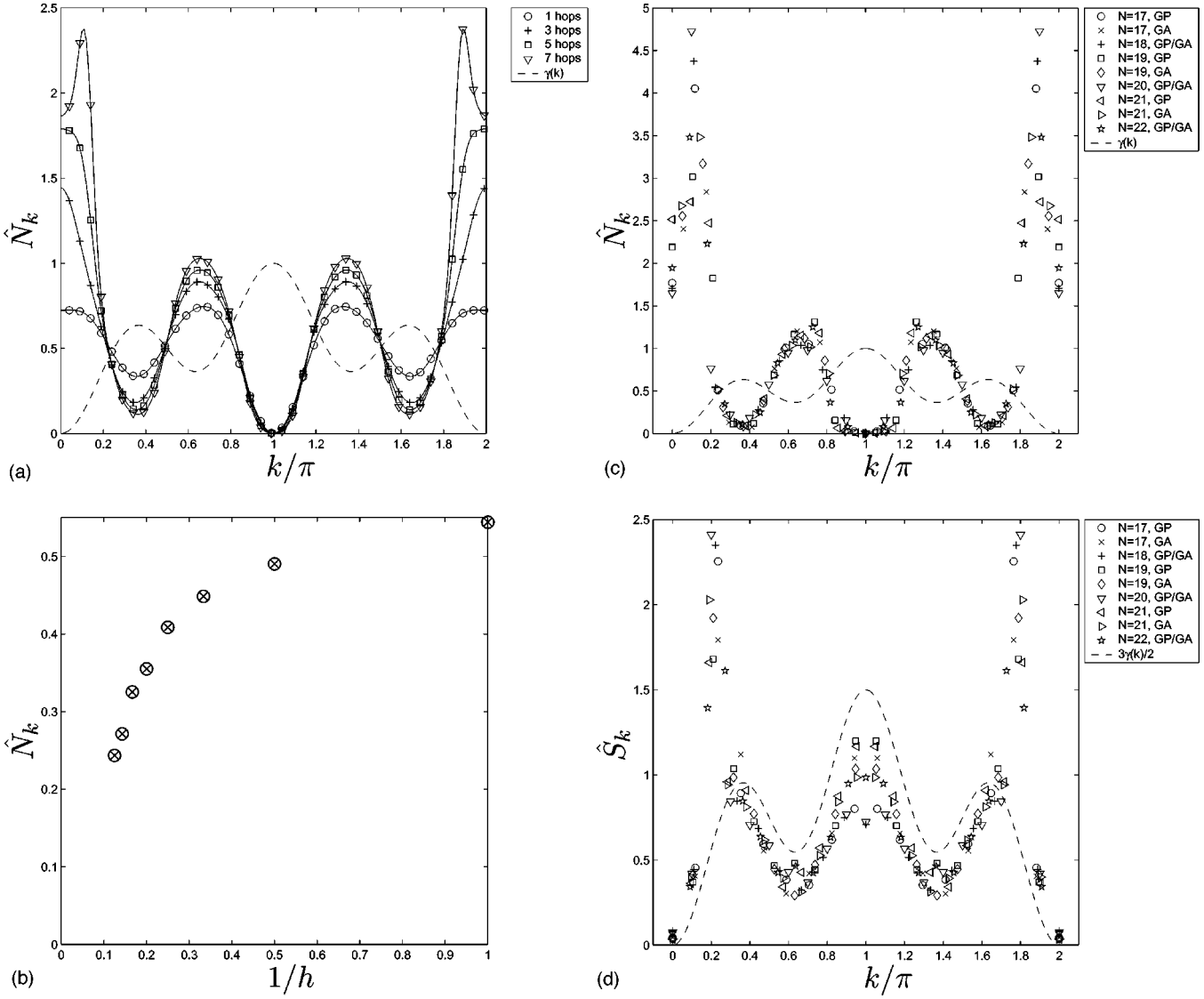

FIG. 17. Correlations on the $p=3$ spiral with periodic local boundary conditions, from (a), (b) semiclassical spiral calculation; (c), (d) finite-size scaled Lanczos calculations. (a) Short-range contribution to $\hat{N}_k$. (b) Long-range contribution to $\hat{N}_k$. (c) Finite-size scaled $\hat{N}_k$. (d) Finite-size scaled $\hat{S}_k$.

correlations are clearly finite, and the system appears to be far from the Fermi-liquid state. The most natural explanation for this result is that the expected small gap in the density of states (DOS) has been filled in, and the state appears to be confined to the linear chain (note the similarity to Fig. 11). The magnetic correlations are well represented by a simple cosine function, suggesting that the correlations are nearest neighbor only.

So far, we have been able to draw apparently reasonable conclusions from the results of these calculations. Naively we conclude that for the locally periodic system, the ground state can be described with a pseudo-Fermi-liquid picture, which would probably degrade into a bosonized Luttinger liquid with power-law divergences if we were to extend the calculation to longer ranges. The locally antiperiodic system appears to prefer the hole motion to be localized along the backbone of the system, and the spin correlations are predominantly nearest neighbor. There is no suggestion of any Fermi-liquid behavior.

However, we have neglected to consider the effect of the global boundary conditions in this analysis. Although the numerical results appear to suggest very good convergence with respect to the global boundary conditions, the results of the calculations on the locally antiperiodic system suggest that the interpretation of these results may be more subtle than we have so far accounted for. The spin correlations shown in Fig. 14(d) suggest that local correlations dominate, indicative of a highly quantum-spin-dimer ground state. The oxygen hole is also known to preferentially form a local singlet, and the resulting motion under our Hamiltonian suggests that the hole can become bound to one or other of the sublattices, as shown in Fig. 15.

For systems with an even number of copper sites, the hole will remain bound to the same sublattice, but an odd number

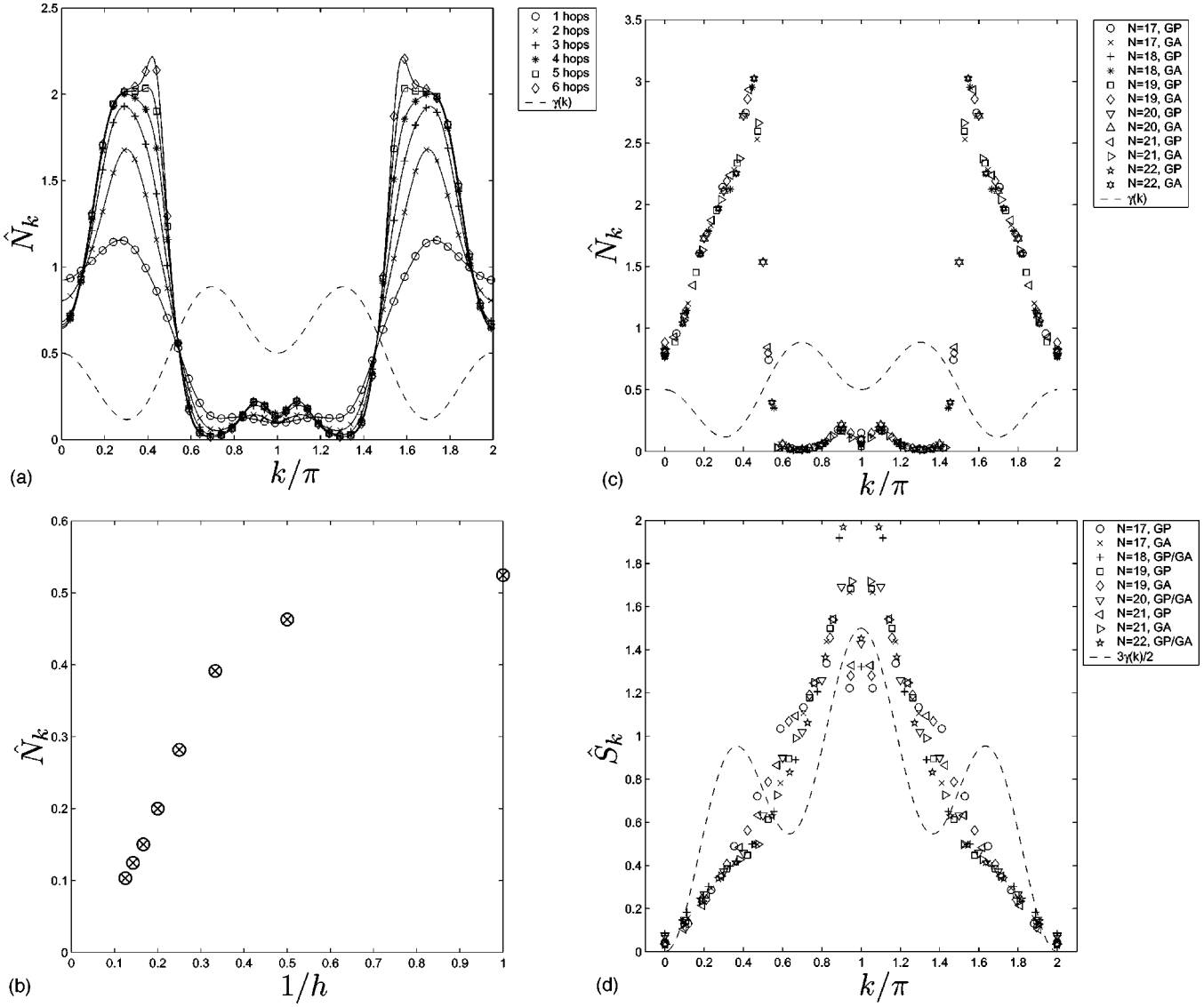

FIG. 18. Correlations on the $p=3$ spiral with antiperiodic local boundary conditions, from (a), (b) semiclassical spiral calculation; (c), (d) finite-size scaled Lanczos calculations. (a) Short-range contribution to $\hat{N}_k$. (b) Long-range contribution to $\hat{N}_k$. (c) Finite-size scaled $\hat{N}_k$. (d) Finite-size scaled $\hat{S}_k$.

of copper sites leads to Möbius boundary conditions, and the hole moves onto the other sublattice. There are hence two possible ground states, one associated with each lattice, and the relative phase of these states is determined by the choice of periodic or antiperiodic global boundary conditions. For periodic boundary conditions, the ground state can be written as $|\psi_p\rangle=|\phi_A\rangle+|\phi_B\rangle$, and for antiperiodic boundary conditions we have $|\psi_a\rangle=|\phi_A\rangle-|\phi_B\rangle$, where $|\phi_A\rangle$, $|\phi_B\rangle$ are the ground states associated with the two sublattices. Adding and subtracting the ground states for the two sets of boundary conditions then allows us to separate $|\phi_A\rangle$ and $|\phi_B\rangle$. In Fig. 16 we show the nearest-neighbor spin correlations as a function of distance from the hole for the two solutions.

It is clear from Fig. 16 that there is a *broken symmetry* in both systems. In the locally periodic system [Fig. 16(a)], the motion of the hole induces spin correlations which optimize its motion. The hole gains most energy from second-neighbor hops and it prefers to be on the oxygen sites on the second-neighbor bonds (note that the correlations for this system are very different to those on the linear chain). When the hole circuits the spiral, the motion is optimized by a locally high-spin state (the oxygen hole unfrustrates each triangle), and the symmetry is broken to allow both of the triangles on which the hole is moving to have high spin. These neighboring pairs of parallel spins then behave like a spin-1 in a Haldane chain-type system. Note that the system is not a pure Haldane chain, and the correlations in Fig. 16(a) are really quite weak. The resulting ground state is hence *not* the pseudo-Fermi liquid we had envisaged, but rather a highly quantum Haldane-like phase, which is somewhat related to a distorted two-component noninteracting Fermi liquid.

The locally antiperiodic system is much more easily interpreted. The correlations shown in Fig. 16(b) suggest an almost pure dimer state, with alternating strong antiferromagnetic and uncorrelated bonds along the chain. The pure

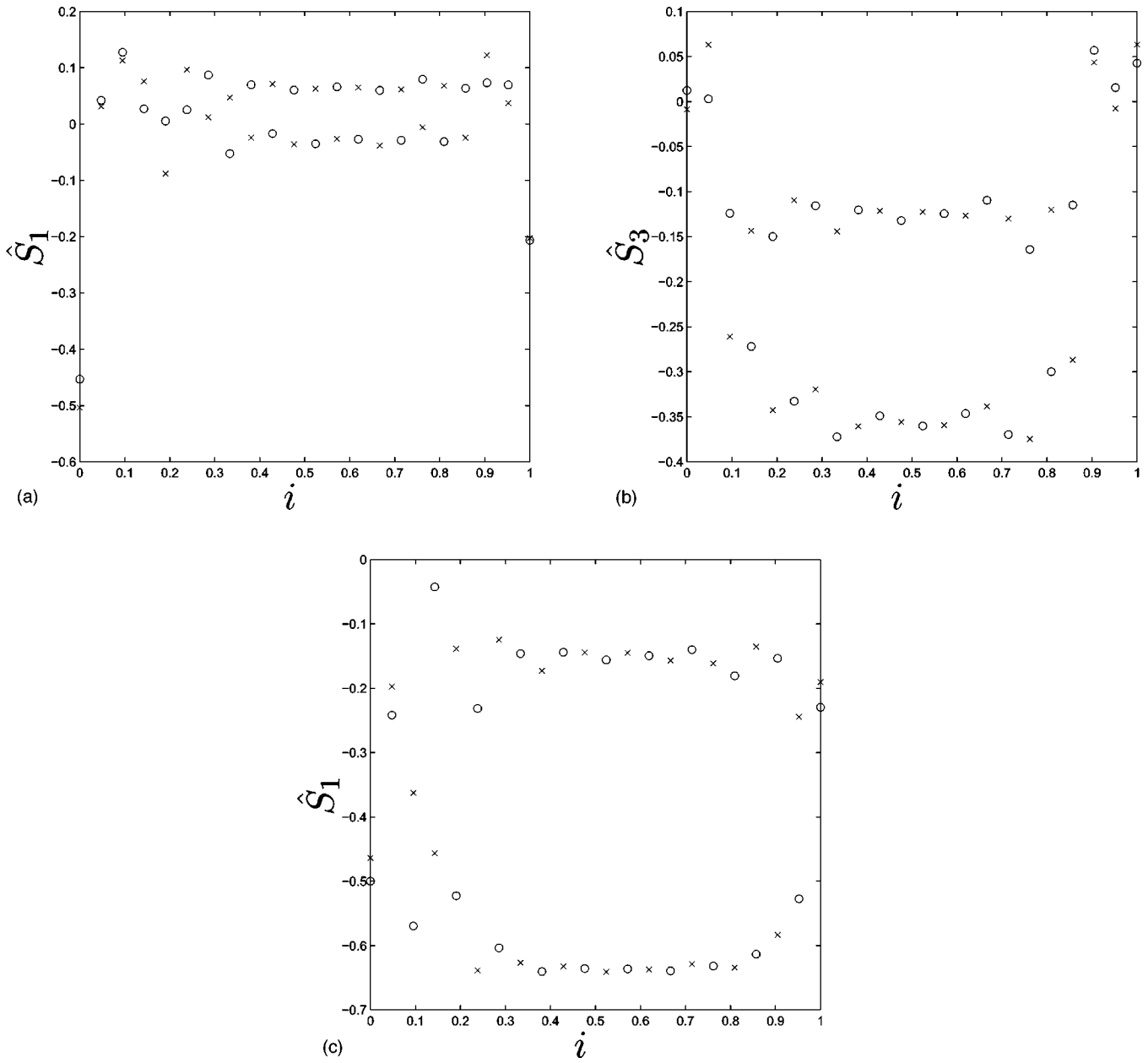

FIG. 19. Spin correlations on the $p=3$ spiral as a function of position on the chain for (a) nearest-neighbor correlations in the locally periodic system, (b) third-nearest-neighbor correlations in the locally periodic system, and (c) nearest-neighbor correlations in the locally antiperiodic system. The two ground states $|\phi_A\rangle$ and $|\phi_B\rangle$ are represented by the symbols $\times$ and $\bigcirc$, respectively.

singlet correlations offer optimal motion around half the triangles, while the other half are essentially irrelevant as the hole is dominantly moving on the backbone of the spiral, not along the second-neighbor bonds. This is basically identical to the predictions made by the t_1-t_2 model[25] on this geometry, which also chooses a dominant sublattice for the charge carrier. Once again, the resulting ground state is strongly quantum and in this case is a simple valence bond solid.

B. $p=3$ spiral

In the Hubbard model framework we would expect the $p=3$ system to differ substantially from the $p=2$ case. The $p=3$ spiral is *bipartite* and would therefore be expected to have a ferromagnetic ground state for the Hubbard model. However, even in the Hubbard framework we find that the two systems are quite similar. The periodic boundary conditions applied to the $p=2$ spiral in the preceding section provided an *unfrustrated* choice of phase for the local hopping which promoted local high-spin correlations. We expect the same to be true for periodic boundary conditions applied to this system, but for antiperiodic boundary conditions to frustrate the system, leading to a low-spin ground state, as we saw for the case of $p=2$. The results for periodic boundary conditions are shown in Fig. 17.

The ground state is indeed low spin and the motion around the bipartite loops is dominated by the process which allows copper-copper singlets to become active Zhang-Rice

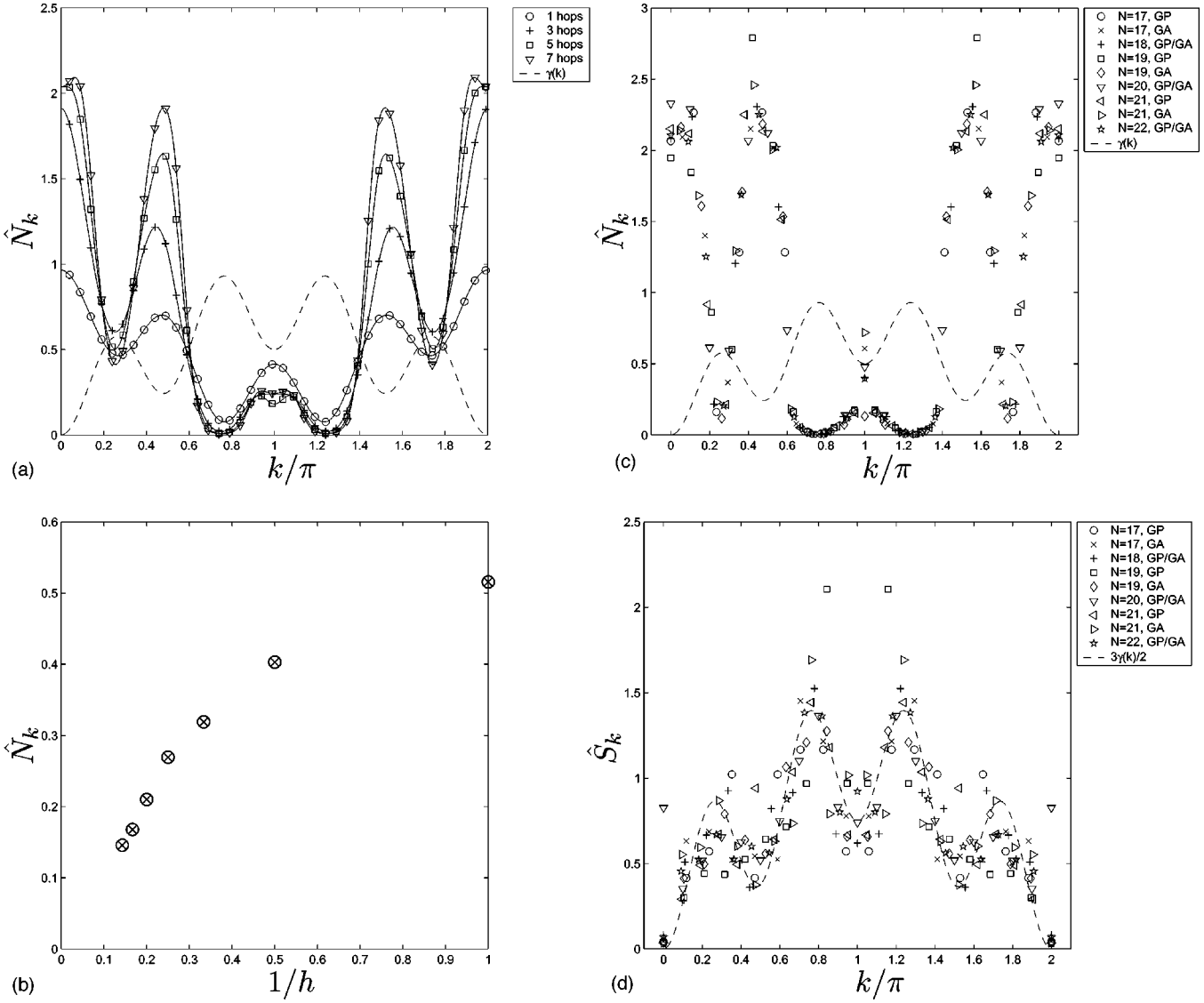

FIG. 20. Correlations on the $p=4$ spiral with periodic local boundary conditions, from (a), (b) semiclassical spiral calculation; (c), (d) finite-size scaled Lanczos calculations. (a) Short-range contribution to $\hat{N}_k$. (b) Long-range contribution to $\hat{N}_k$. (c) Finite-size scaled $\hat{N}_k$. (d) Finite-size scaled $\hat{S}_k$.

singlets. In the Fermi-liquid picture we expect six Fermi points, with a small Fermi sea centered on the origin filled to $k=\pm\pi/4$ and two symmetrically related filled regions between $\pm\pi/2$ and $\pm 3\pi/4$. A Bragg spot would be expected at $k^*=\pi/4$, which is close to the observed behavior but does not accurately describe the system. There is a small patch of filled Fermi sea close to the origin which is bound by strong divergences which are either power-law divergent or converge on a length scale of tens of unit cells. The magnetism is consistent with the nesting vector across this region.

The results for locally antiperiodic boundary conditions are shown in Fig. 18. They are very similar to those of the $p=2$ spiral, with the number correlations very like those of the linear chain, and the spin correlations are short-range. There are minor differences, such as the small occupied region near the origin [Fig. 18(c)]. Most importantly, the long-range contribution clearly vanishes, and we do not have a Fermi-liquid state. As we saw for the $p=2$ spiral, there is a clear broken symmetry, illustrated by the spin correlations shown in Fig. 19. The antiperiodic system exhibits a clear dimerization, while the periodic system also displays a weakly broken symmetry which is clearest when examining the third-neighbor correlations shown in Fig. 19(b) (the system has a direct bond between third nearest neighbors). Both systems have a quantum ground state which appears to be a valence bond solid. In addition, the hole appears to act as a domain wall, as was the case for $p=2$. This is expected to become less important as we move towards two dimensions.

C. $p=4$ spiral

We now move on to analyze the case $p=4$. The loops of the spiral are now *pentagonal* and are longer than the loops of the underlying square lattice and should consequently be less influential. Each section of the spiral has an odd number of sites and so a hole moving around the small loop can have

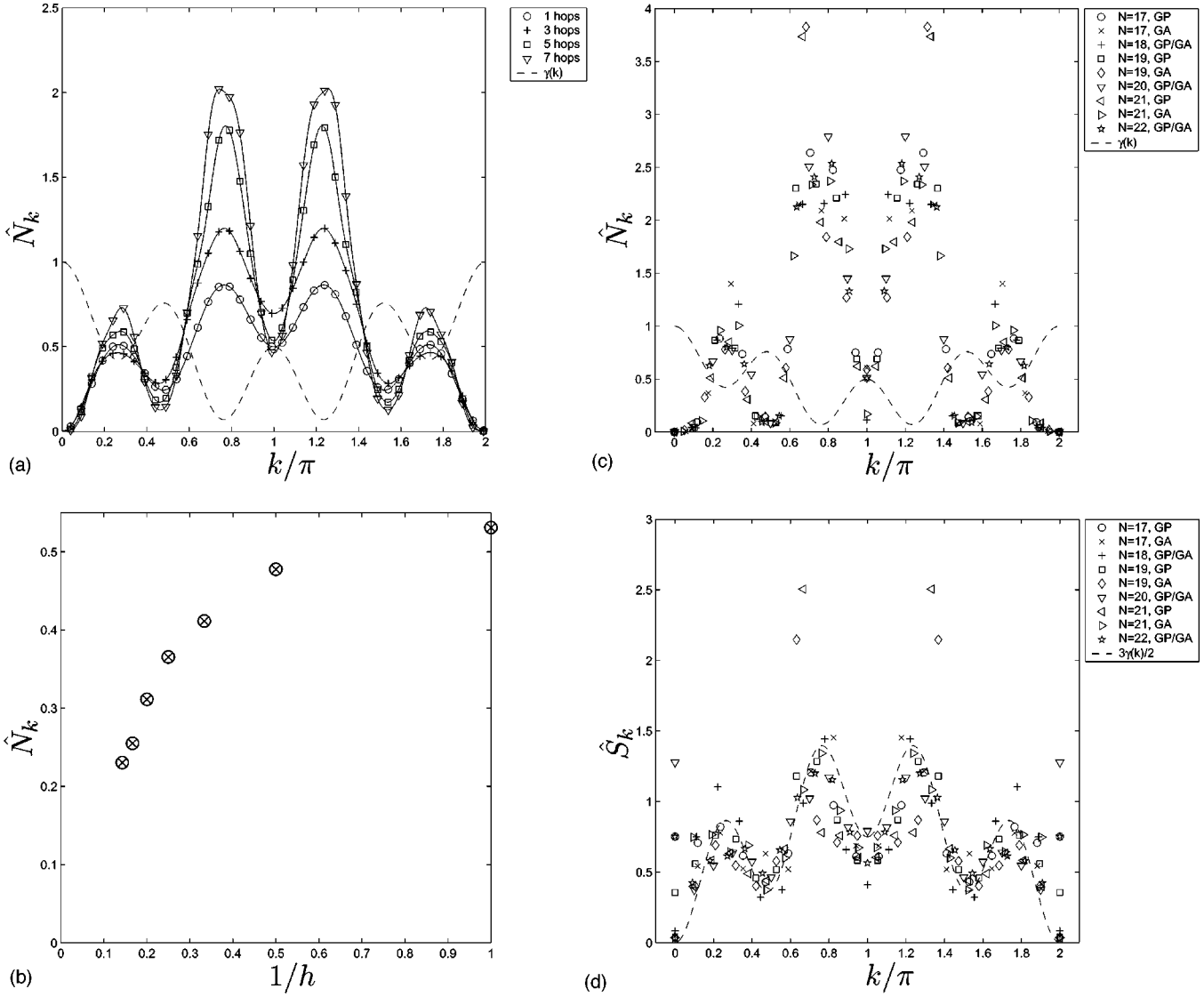

FIG. 21. Correlations on the $p=4$ spiral with antiperiodic local boundary conditions, from (a), (b) semiclassical spiral calculation; (c), (d) finite-size scaled Lanczos calculations. (a) Short-range contribution to $\hat{N}_k$. (b) Long-range contribution to $\hat{N}_k$. (c) Finite-size scaled $\hat{N}_k$. (d) Finite-size scaled $\hat{S}_k$.

an unfrustrated phase with local periodicity and a frustrated phase with local antiperiodicity. The noninteracting solution has eight Fermi points located at

$$k \approx 0.204\pi,\ 0.3288\pi,\ 0.6024\pi,\ 0.9777\pi, \qquad (45)$$

and their reflections about $k=\pi$. The results for the locally periodic boundary conditions are given in Fig. 20. The occupied regions are consistent with the Fermi picture, and the long-range contribution disappears quickly. The underlying background is smooth, and there is no evidence for any kind of divergence in the occupation number. The spin correlations almost exactly mirror the structure factor scaled to area $s(s+1)=3/4$ and correspond to essentially pure nearest-neighbor spin correlations. This state does *not* display the broken symmetry we have seen in previous systems and has the characteristics of a resonating valence bond state,[28] a truly quantum phase.

The $p=4$ system with locally antiperiodic boundary conditions (Fig. 21) is surprisingly similar to the periodic system. The occupied regions mirror the noninteracting solution, with the exception of a small region close to $k=\pi$ which is unexpectedly filled. The spin correlations once again are well described by the scaled structure factor and offer the same RVB state as the periodic system, with no evidence for a broken symmetry or a domain wall formed by the hole. Note that this equivalence of boundary conditions is indicative of the thermodynamic limit being approached.

D. $p=5$ spiral

The final system we will examine is the $p=5$ spiral. Although this is the most relevant system with regard to convergence toward two dimensions, as we have already discussed, we are unable to solve systems large enough to converge. This is an unfrustrated system with ten Fermi

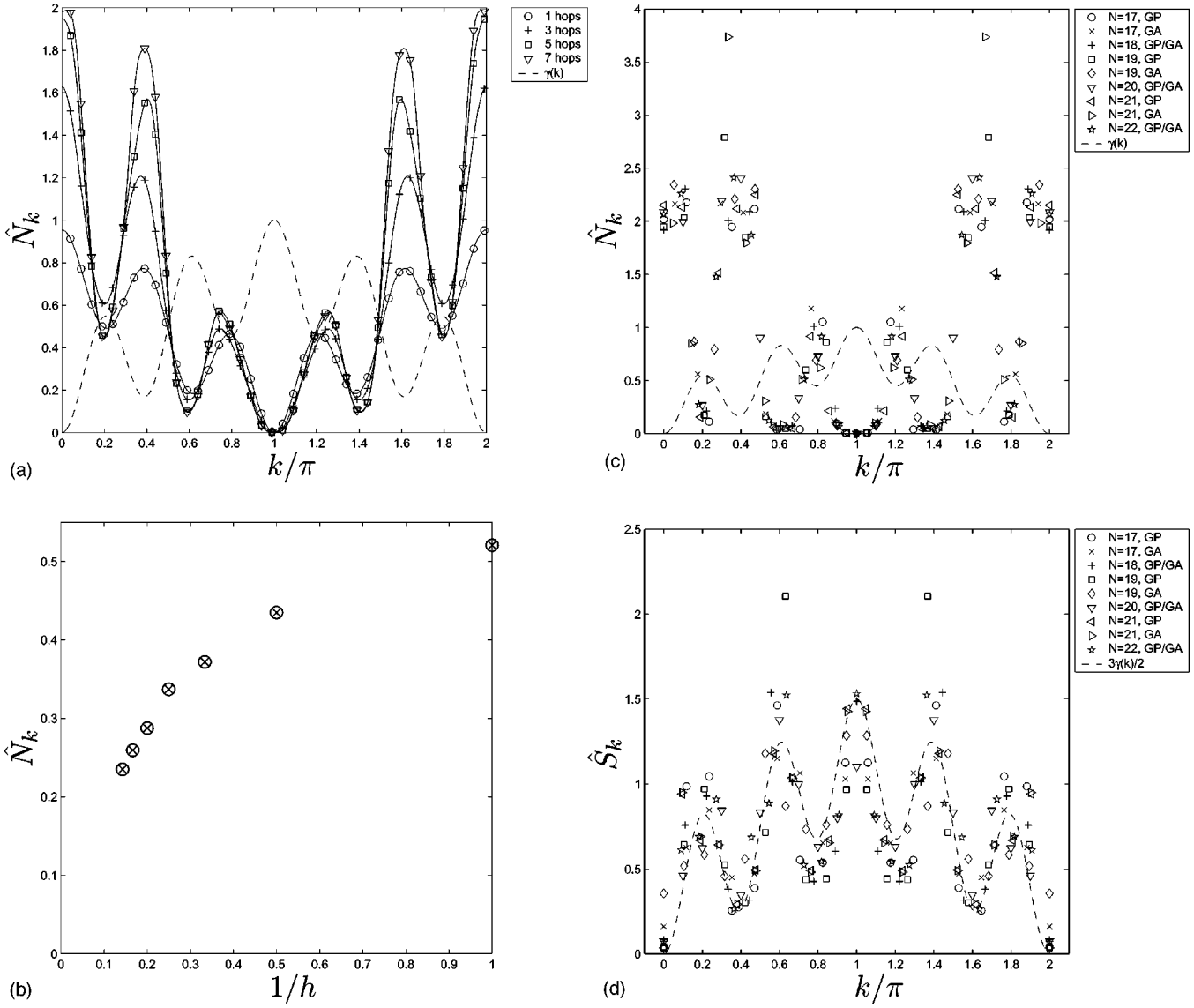

FIG. 22. Correlations on the $p=5$ spiral with periodic local boundary conditions, from (a), (b) semiclassical spiral calculation; (c), (d) finite-size scaled Lanczos calculations. (a) Short-range contribution to $\hat{N}_k$. (b) Long-range contribution to $\hat{N}_k$. (c) Finite-size scaled $\hat{N}_k$. (d) Finite-size scaled $\hat{S}_k$.

points at $k=\pi/6, \pi/4, \pi/2, 3\pi/4, 5\pi/6$ and their reflections through $k=\pi$. The behavior is now complicated, and the data appear quite ragged and hence are difficult to interpret. The results for the locally periodic system are shown in Fig. 22.

The results for the periodic system are very similar to those obtained for $p=4$, with only nearest-neighbor spin correlations observed and no divergence in $\hat{N}_k$, although the occupied regions are broadly consistent with the noninteracting solution. The antiperiodic system (Fig. 23) displays essentially the same behavior. There is no broken symmetry evident for either system and little dependence on the global boundary conditions. The equivalence of the two types of local boundary condition suggests that the spiral loops may be longer than the correlation length and the calculations have converged.

The final task in the finite-size scaling analysis of this section is to consider the sequence of converged systems as a function of p and identify a pattern. The earlier systems in the sequence were seen to be strongly dependent on local boundary conditions and exhibited quantum states characterized by a broken symmetry and a spinon bound to the hole. The broken symmetry vanishes at $p \geqslant 4$ and leaves a quantum state that is essentially comprised of resonating valence bonds. In a related paper[27] it has been shown using these techniques that the t model on the triangular lattice is predicted to have an ordered three-sublattice 120° antiferromagnetic ground state, which is simultaneously a single-component Fermi liquid. This implies that the techniques we have used are capable of identifying classical and quantum states and that any bias towards one or the other is small.

E. Square lattice

In the previous sections we have performed both semiclassical spiral calculations on infinite systems and quantum

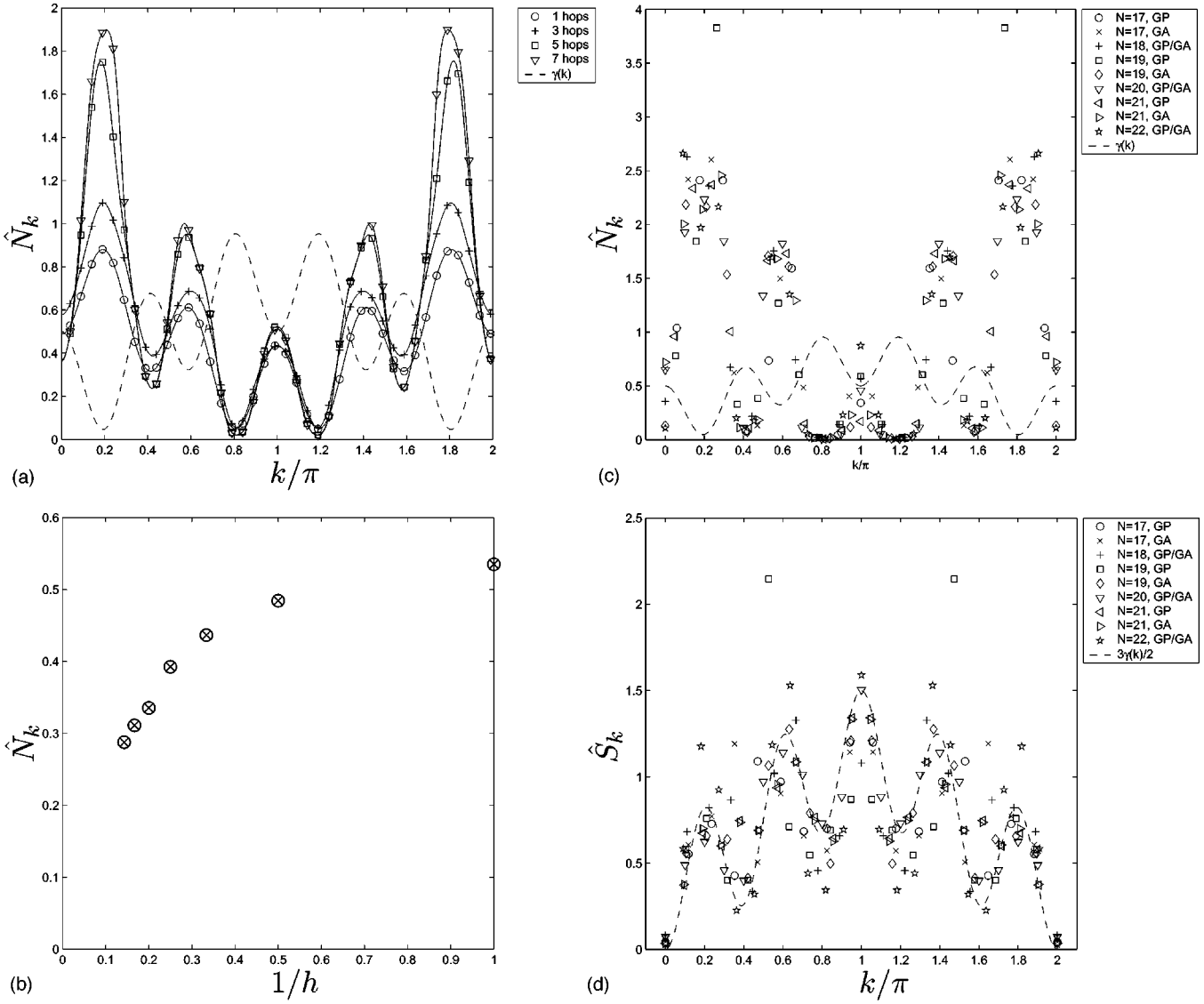

FIG. 23. Correlations on the $p=5$ spiral with antiperiodic local boundary conditions, from (a), (b) semiclassical spiral calculation; (c), (d) finite-size scaled Lanczos calculations. (a) Short-range contribution to $\hat{N}_k$. (b) Long-range contribution to $\hat{N}_k$. (c) Finite-size scaled $\hat{N}_k$. (d) Finite-size scaled $\hat{S}_k$.

numerical calculations on a series of systems which limit to the CuO_2 lattice. An examination of the occupation numbers predicted by these calculations suggests that the semiclassical approach can be consistent with the numerical calculations. Ultimately, we would like to be able to study the square lattice in detail. Numerically, this is not possible as we are restricted to low values of N and, hence, low values of p, but having established the consistency of our two approaches, we can use the semiclassical technique to study the square lattice directly.

We first calculate the preferred pitch of the classical spiral, which, as p becomes large, can be seen to converge towards the commensurate position, $q=(2\pi/3)(1,1)$, the classical 120° phase usually associated with the triangular lattice, and a type of three-sublattice antiferromagnet. This is depicted in Fig. 24.

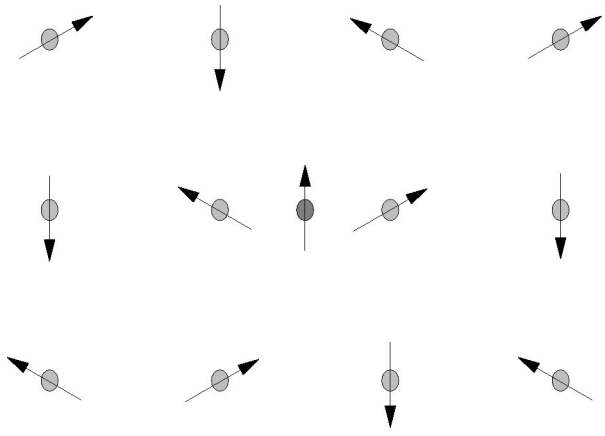

FIG. 24. The preferred two-dimensional classical spiral.

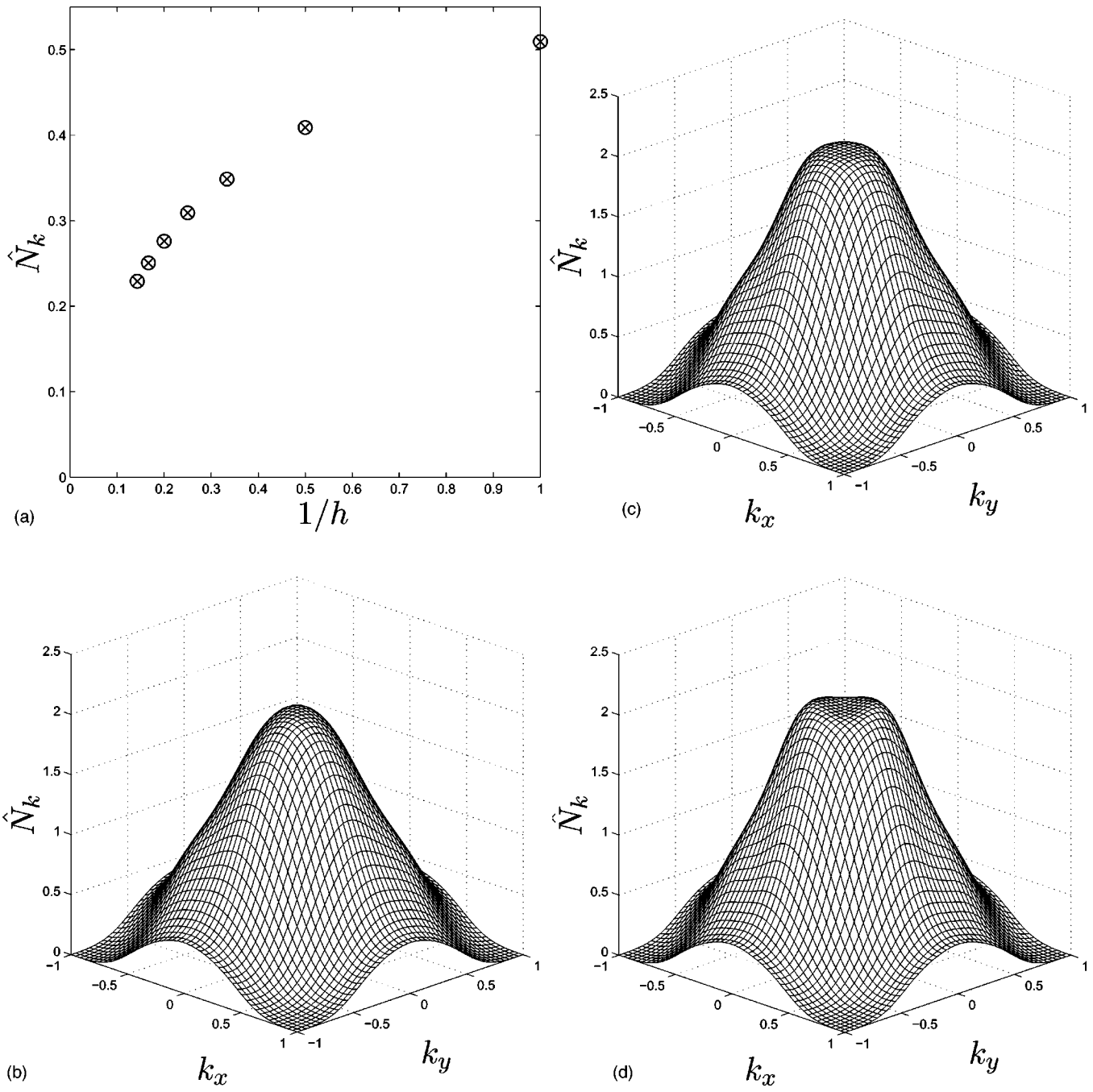

FIG. 25. Occupation number correlations on the square lattice. (a) Long-range contribution. (b) Short-range contributions including six hops. (c) Short-range contributions including seven hops. (d) Short-range contributions including eight hops.

Using this knowledge, we can calculate full two-dimensional wave functions, yielding the results shown in Fig. 25. The long-range contribution to the occupation number decays quite rapidly, and its weight is distributed smoothly into the short-range contribution. The calculations which include the most hops indicate a "flat top" with a well-defined rim and a slight indentation, but there is no evidence for a divergence. The noninteracting Fermi surface is the square connecting the midpoints of the sides of the Brillouin zone, and although the smooth peak respects this line, the expected divergence in $\hat{N}_k$ is not located on this Fermi surface and has no remnant in the short-range contribution.

VI. CONCLUSIONS

In this paper we have studied a restricted limit of a fairly simple model which is of relevance to the cuprate superconductors. We make two main assumptions when developing our model. First, we assume that behavior of the cuprates is controlled by the chemical bonding, and we do not include other types of coupling—e.g., phonons, plasmons, excitons,

etc. This leads us to study the three-band model, which is the standard starting point for the cuprates. Our second main assumption is that the charge degree of freedom on the copper ions is frozen, consistent with the known Mott insulating behavior. This permits the reduction of the three-band model to the *t*-*X* model, to which can be added direct oxygen-oxygen hopping t_p and/or a Heisenberg interaction *J*. These terms are intrinsically *smaller* than *t* and *X*, and we choose not to include them. A popular method of approaching this model is to reduce it to the *t*-*J* model using the concept of a Zhang-Rice singlet[1] to project out the oxygen states, leaving only the copper square lattice. This corresponds to the dominance of Cu^{3+} in the intermediate state for fluctuations, which is not seen experimentally. We choose to study the opposing limit of Cu^{+} dominance, which is physically relevant and provides the *X*-*J* model.

The *t*-*J* model and the *X*-*J* model are both beyond the scope of current techniques to allow us to gain a clear understanding of either model, but there are some limits in which progress may be made. In this article we have studied the motion of a single hole in the limit of vanishing *J*, leaving only the *X* model. Although we have not presented the evidence here, the inclusion of *t* permits the one-hole problem to exhibit a first-order transition from a ferromagnetic ground state at $t/X=1$ (corresponding to Nagaoka's ferromagnetism[20]) to a sophisticated low-spin ground state at $t/X=0$, which is the subject of this work. The real physical system has $t/X\approx 0.2$, which is *below* the transition to the high-spin ground state. We also wish to point out that the low-spin ground state which our calculations suggest will be stabilized further by the inclusion of the ubiquitous superexchange interaction present in the real system. This is in contrast to the *t*-*J* model where the hole motion and superexchange are in direct competition.

We have utilized two separate techniques to study a sequence of geometries which limit to the CuO_2 lattice. Our chosen methods are (i) exact diagonalization via the Lanczos algorithm and (ii) classical spin spirals plus quantum fluctuations. The computational limitations imposed by the Lanczos algorithms provide a severe restriction on the size of systems we can study and we are limited to studying spiral geometries with pitch $p\leqslant 5$. We are able to compare the two approaches, and we find that the semiclassical approach can be consistent with exact diagonalization, in that the occupation numbers predicted by both techniques are consistent, although some care is required. We also note that systems with small values of *p* are tractable, but are not necessarily representative of the large-*p* limit, corresponding to the square lattice of interest.

All of our calculations suggest a strongly quantum solution, characterized by dominant nearest-neighbor spin singlets between copper local moments. The nearest classical state is not magnetic, but is the noninteracting half-filled solution of the Hubbard model: the filled regions (*consistent with the expected large Fermi surface*) observed in our calculations usually mirror those of the noninteracting solutions, although the anticipated Fermi discontinuities are replaced by a smooth transition between filled and unfilled regions. The tightest spirals we studied yielded a broken symmetry, where the preferred valence bonds become localized, forming a valence bond solid which ties the Zhang-Rice singlet onto one of the two sublattices, promoting motion around only half of the available loops. As the spiral is extended, this broken symmetry is lost, and the valence bonds "melt" to form a type of resonating valence bond state.

We also briefly studied the square lattice problem directly using the semiclassical technique. These calculations suggest the absence of a divergence in $\hat{N}_k$, indicating that the system does not exhibit Fermi-liquid behavior.

In summary, we believe that a single hole in the *X* model yields an interesting low-spin quantum ground state. This state is *not* a Fermi liquid and is best described as a resonating valence bond state. Further investigation is required in order to determine the effect of introducing additional holes, which we have not attempted in this work.

ACKNOWLEDGMENTS

We wish to acknowledge useful discussions with C. Hooley. I.B.S. wishes to thank the EPSRC for financial support.

[1] F. C. Zhang and T. M. Rice, Phys. Rev. B **37**, 3759 (1988).
[2] J. R. Schrieffer, X. G. Wen, and S. C. Zhang, Phys. Rev. B **39**, 11 663 (1989).
[3] S. R. White and D. J. Scalapino, Phys. Rev. B **55**, 6504 (1997).
[4] V. J. Emery and S. A. Kivelson, Physica C **209**, 597 (1993).
[5] D. Emin, Phys. Rev. Lett. **62**, 1544 (1989).
[6] I. B. Styles and M. W. Long, J. Phys. A **36**, 9361 (2003).
[7] V. J. Emery, Phys. Rev. Lett. **58**, 2794 (1987).
[8] G. Aeppli, S. M. Hayden, H. A. Mook, Z. Fisk, S.-W. Cheong, D. Rytz, J. P. Remeika, G. P. Espinosa, and A. S. Cooper, Phys. Rev. Lett. **62**, 2052 (1989).
[9] S. M. Hayden, G. Aeppli, R. Osborn, A. D. Taylor, T. G. Perring, S. W. Cheong, and Z. Fisk, Phys. Rev. Lett. **67**, 3622 (1991).
[10] Y. Tokura, S. Koshihara, T. Arima, H. Takagi, S. Ishibashi, T. Ido, and S. Uchida, Phys. Rev. B **41**, 11 657 (1990).
[11] M. Greven, R. J. Birgeneau, Y. Endoh, M. A. Kastner, B. Keimer, M. Matsuda, G. Shirane, and T. R. Thurston, Phys. Rev. Lett. **72**, 1096 (1994).
[12] D. Salamon, R. Liu, M. V. Klein, D. A. Groenke, K. R. Poeppelmeier, B. Dabrowski, P. D. Han, and D. A. Payne, Phys. Rev. B **47**, 12 242 (1993).
[13] M. Rubhausen, N. Dieckmann, A. Bock, U. Merkt, W. Widder, and H. F. Braun, Phys. Rev. B **53**, 8619 (1996).
[14] R. Coldea, S. M. Hayden, G. Aeppli, T. G. Perring, C. D. Frost, T. E. Mason, S.-W. Cheong, and Z. Fisk, Phys. Rev. Lett. **86**, 5377 (2001).
[15] B. O. Wells, Z.-X. Shen, A. Matsuura, D. M. King, M. A. Kastner, M. Greven, and R. J. Birgeneau, Phys. Rev. Lett. **74**, 964

(1995).
[16] S. Uchida, T. Ido, H. Takagi, T. Arima, Y. Tokura, and S. Tajima, Phys. Rev. B **43**, 7942 (1991).
[17] J. R. Schrieffer and P. A. Wolff, Phys. Rev. **149**, 491 (1966).
[18] A. Fujimori, E. Takayama-Muromachi, Y. Uchida, and B. Okai, Phys. Rev. B **35**, 8814 (1987).
[19] N. Nücker, J. Fink, J. C. Fuggle, P. J. Durham, and W. M. Temmerman, Phys. Rev. B **37**, 5158 (1988).
[20] Y. Nagaoka, Phys. Rev. **147**, 392 (1966).
[21] A. Ino, C. Kim, T. Mizokawa, Z. X. Shen, A. Fujimori, M. Takaba, K. Tamasaku, H. Eisaki, and S. Uchida, J. Phys. Soc. Jpn. **68**, 1496 (1999).
[22] J. D. Champion and M. W. Long, J. Phys. A **36**, 9351 (2003).
[23] T. Holstein and H. Primakoff, Phys. Rev. **58**, 1098 (1940).
[24] M. W. Long, J. Phys.: Condens. Matter **4**, 3235 (1992).
[25] M. W. Long, C. W. M. Castleton, and C. A. Hayward, J. Phys.: Condens. Matter **6**, 9359 (1994).
[26] J. M. Luttinger, Phys. Rev. **119**, 1153 (1960).
[27] M. W. Long and M. R. Harvey (unpublished).
[28] P. W. Anderson, Science **235**, 1196 (1987).